Lessons in Nanotechnology from
Traditional and Advanced Ceramics
J.-F. Baumard (Editor)

COLLOIDAL LESSONS LEARNED FOR DISPERSION OF NANOSIZE PARTICULATE SUSPENSIONS

James H. ADAIR

with contributions from
Rajneesh KUMAR, Nicolas ANTOLINO, Christopher SZEPESI,
R. Allen KIMEL, and Sarah M. ROUSE
NSF Particulate Materials Center, Materials Research Institute,
Materials Science & Engineering, The Pennsylvania State University,
University Park, PA, USA

The formation of stable, unagglomerated nanocolloids for a variety of applications is the critical issue to be addressed if the potential of these materials is to be achieved. Fundamental concepts in colloid and interfacial chemistry can be adapted to provide robust, reliable dispersion schemes for nanocolloids. Unique characteristics of nanoparticulates in suspension relative to sub-micron particulates such as the liquid mediated sintering of nanoparticulates at contact points among aggregates must be recognized and colloidal chemistry strategies adopted. Two broad strategies for the successful dispersion of nanoparticulates in liquids have been developed, protection-dispersion and passivation-dispersion. Both strategies recognize the high surface reactivity of nanoparticulates and adapt the colloid and interfacial chemistry to mitigate the tendency for liquid phase sintering at the contacts among aggregated materials.

Three examples of protection-dispersion and passivation-dispersion for nanocolloids are presented. For the first time, it is shown that stress corrosion cracking concepts can be used to promote the de-aggregation of a vapor phase synthesized and heat treated nanophase, nanocrystalline ceramic, a powder composed of mixed phases of alumina. Chemically aided attrition milling (CAAM) has been used to reduce the particle size distribution to the nanoscale with 100% of the material after one hour of milling below 500nm and 90% in the range of 30nm. Critical milling variables have been examined and discussed for the CAAM process including solution pH and material solubility, zeta potential and degree of dispersion with milling. The chemical synthesis of yttrium doped zirconia via a hydrothermal route with recovery and subsequent processing to bulk ceramics has also been discussed. The process depends on the specific use of protection-dispersion during synthesis

based on the zirconium-bicine metal ligand complex and passivation-dispersion based on the zirconium-oxalate metal ligand complex to prepare well-dispersed, concentrated suspensions. Finally, for the first time, nanocomposite colloids, prepared using a protection-dispersion scheme, have been described that have the potential for bio-imaging as well as drug and gene therapies. The critical element in the nanocomposite particulate dispersion for nanomedical applications is the combination of protection-dispersion based on the amphiphile-dispersant combination combined with careful particulate laundering and dispersion using high-performance liquid chromatography technique adapted for the nanocolloids. Thus, sound colloidal principles can be used to create well-dispersed nanocolloids if the unique colloidal characteristics of nanoparticulates are recognized and accommodated during processing.

1. INTRODUCTION AND OBJECTIVES

Colloid and interfacial chemistry has a well-deserved reputation of providing guidance in the dispersion of particles in liquids. Yet there have been no systematic studies reporting the dispersion of nanometer scale particulates in liquids.* The intent of this document is to review the fundamental features of suspensions composed of nanoscale particulates relative to the science and technology associated with larger particulates in aqueous suspension and to discuss where these principles have been used to provide robust dispersion strategies for selected examples of nanoparticulates. Macroscopic particulate dispersion has been reviewed by a great number of excellent treatises to provide the basic knowledge relative to the dispersion of macroscopic powders in liquids.[1-29] Some of the most useful references related to nanoparticulate synthesis and dispersion in the earlier reports are from Faraday in the 1850's and proceed up to the 1950's.[2-8] Many of these early texts, especially those of Faraday, Zsigmondy, Svedberg, and Kruyt, have addressed in addition to the relevant scientific principles known at the time, the general engineering issues associated with preparing stable nanocolloids.[2-5] More recently, colloidal phenomena has aroused great interest from the ceramic community because of the need to manage agglomeration.[30-44] However, all of the ceramic efforts to date have been directed toward submicron and larger particulate sizes. Nonetheless, there is a large literature developed over the past 150 years that can be used for guidance in the dispersion of nanoscale particulates in colloidal suspension.

** For the sake of this report, nanometer scale particulates are those with at least one dimension less than 50nm. As a consequence, particles greater than 50nm are considered macroscopic particulates.*

There are two broad approaches to dispersing nanoscale powders in liquids that depend on the source and nature of the nanoscale powder. Most commercial nanoscale powders are synthesized through vapor phase processes. Vapor phase synthesized powders are invariably agglomerated and must be de-agglomerated to be of use in the preparation of bulk materials. In contrast, many material systems are amenable to precipitation from solution. For solution synthesized particulates, the issue is to maintain the particles in a well-dispersed state during the washing, collection, and concentration steps subsequent to particle formation. Basic concepts in colloid and interfacial chemistry can be applied to achieve the goal of well-dispersed particulates for the two general classes of powders.

The world wide market impacted by particulates was over $1 trillion (US) based on 1993 US Department of Commerce estimates.[31] Almost a third of this market is found in chemical and allied products, most of which are related to catalyst applications of fine particulates. The majority of powders for catalytic applications are prepared through vapor phase reactions. Catalytic powders are nanometer scale particulates that are intentionally agglomerated to minimize dusting of the nanoscale particulates. Thus, there is already a large quantity of nanoscale particulates produced by the catalytic industry, but not in form suitable for ceramic powder processing to bulk materials.

What are the powder characteristics desired to process bulk materials? Messing has addressed these issues for sub-micron powders typical of ceramics:[32]

1. Particle size between 0.1 and 1.0 μm diameter. The upper size limit is established by thermodynamics of sintering. The lower size limit is set by need to avoid particle agglomeration.
2. Broad particle size distribution resulting in a narrow pore size distribution of small pores (i.e. <50 nm) and maximum packing density. A broad particle size distribution leads to increased packing density and less sintering shrinkage. A small pore size leads to decreased sintering distance and, consequently lower temperature
3. Equiaxed particle shapes are required to achieve the most uniform packing and highest packing density. One must avoid particle shape induced anisotropic shrinkage.
4. Dense particles are required to achieve the minimum shrinkage requirement.
5. No powder defects (e.g. agglomerates, aggregates). Agglomerate mediated defects destroy the benefits of 1-4.

Of the various desirable characteristics, well-dispersed or dispersible particulates are the key element as the presence of agglomerates compromises all other desirable characteristics. Thus, a critical element, generally ignored,

is to address the processing required to eliminate or at least reduce the deleterious effects of agglomeration. Based on the two general classes of powders, the following questions must be addressed if nanoscale particulates are to achieve their potential in the manufacture of bulk materials:

1. *For vapor phase particulates, can the nanoscale aggregates typically present in these powders be reduced to nanoscale primary particles?*
2. *For solution synthesized particulates, can nanometer size particles be chemically synthesized and recovered in a well-dispersed state in commercial quantities with at least a minimum yield equal to 10 weight percent of the total synthesis volume?*

The first question addresses the fundamental limitation embedded in the dogma associated with milling, that it is impossible to reduce particulates below about 1 micron.[44] There have been various rationales for this dogma including arguments that the defect concentration diminishes dramatically for material scales below 1 micron, therefore drastically limiting particle size reduction through crack propagation in brittle materials. As will be shown in the current report, another mechanism has been developed that takes advantage of another crack propagation phenomena, stress corrosion cracking along the grain boundaries of polycrystalline aggregates typical of vapor phase synthesized, nanoscale powders.

The second question addresses the critical issue associated with solution synthesized particulates. Can enough material be produced that meets each of the five Messing criteria for feasible, much less commercial, processing of bulk materials? By maintaining very low particulate numbers via low super-saturations, it is possible to produce nanoscale, apparently well-dispersed nanoscale particulate via solution approaches. Unfortunately, the low yields prohibit the production of bulk materials beyond a few dozen milligrams, much less the desirable gram to kilogram quantities required for a single part. It will be shown that there are multiple strategies discussed in the literature that provide both excellent material yield and good dispersion.

This report is organized around four sections: the introduction and a review of the relevant colloidal chemistry and the impact of nanoscale particulates on these fundamental principles; a milling approach based on the concept of chemically aided attrition milling (CAAM) that permits the breakdown of polycrystalline alumina agglomerates to nanoscale particulates; a protection-dispersion approach that enables the production of high yields of well-dispersed, solution synthesized yttria tetragonal zirconia (TZP), and the protection-dispersion approach that permits the preparation of nanocomposite silica and other material-based nanoparticulates for nanomedical applications including bioimaging and, potentially, drug and gene therapy via nanoparticulate delivery systems.

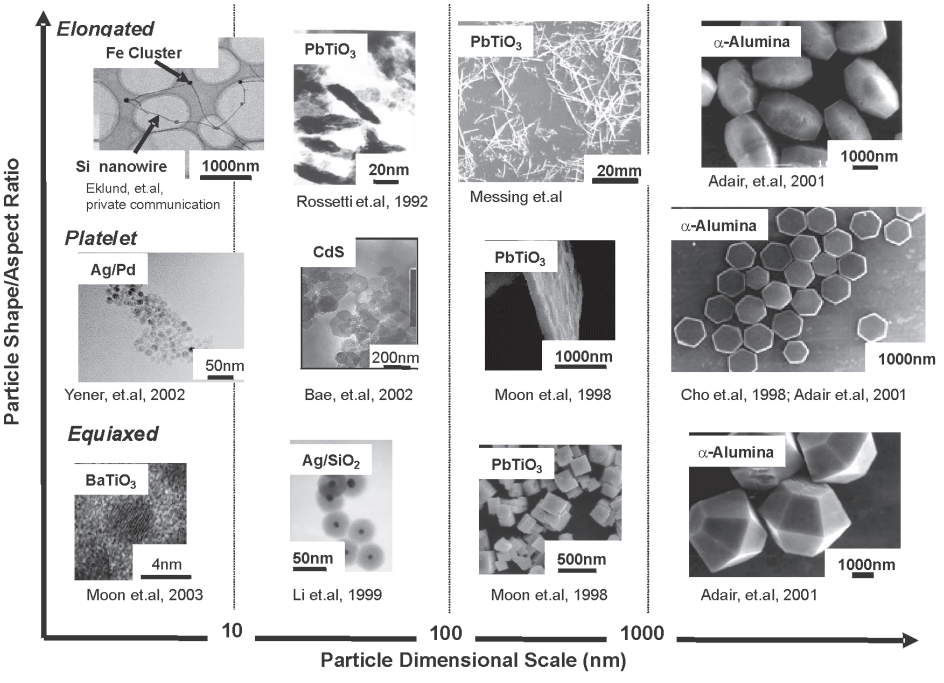

FIGURE 1.1 - Designer particles as a function of scale and aspect ratio created by Penn State Particulate Materials Center faculty and collaborators.

1.1. Principles for dispersion of nanoscale colloids

The elegance and beauty of particulates from the nanoscale to the macroscale as a function of morphology are displayed in Figure 1.1. Unfortunately, the utility of these interesting and sometimes, unique particulates is compromised if the forces driving the particles together into irreversible agglomerates are not addressed. The issues associated with the dispersion of sub-micron and larger particles in liquids are well-established (see for example, Hunter,[18]). The features associated with dispersion of macroscopic particulates and those particular to nanoscale particulates are summarized in Table 1.1. Each of these will be addressed in the following sections.

1.1.1. Phase stability and solution ionic equilibria

While the phase stability for many materials in water is known, it is generally ignored or simply not appreciated.[21,22,25,27,30,39,41,44] The thermodynamically stable material, particularly in an aqueous environment, is not

TABLE 1.1 - Comparison of macro- and nano-scale particulate dispersion.

Macroscopic Particulate	Nanoscale Particulate
Phase stability known, but usually not appreciated	Surface reactions dictate phases present
Solution Ionic Equilibria	Yes, but…. Ostwald-Freundlich → Elevated Solubility
Zeta Potential and Surface Charging Mechanisms	Yes, but…. Little is known at the nanoscale
Influence of Hamaker constant well established (e.g, French et.al, & Bergstrom)	May scale with size, even have fundamental changes in relationships
Polymeric flocculation to concentrate/wash particles	Low charge, small adsorbates
Protective colloids Fairly general	Requires specific complexing agents
Polyelectrolyte dispersion Generic dispersants	Highly charged, surface complexing agents Requires specific complexing agents

usually the phase one thinks of as our ceramic.[41] For particulates greater than 1 micron, surface reactions leading to the typical hydrated or carbonated stable phase, are not severe enough to compromise processing or ultimate properties in dense ceramics. In the case of nanoscale particulates the entire material may devolve into the thermodynamically stable phase. For example, in Figure 1.2, the species predominance diagram for the Ba-Ti-CO_2-H_2O system is shown.[41] The solubility of the Ba^{2+}(aq) for the 'Virgin $BaTiO_3$' generally agrees with that of $BaCO_3$ over most of the suspension pH range evaluated. The large change in solubility and the depleted Ba zone shown in the TEM photomicrograph lead to agglomeration as well as abnormal grain growth because of Ti-rich regions that promote liquid phase formation. Fortunately, when the phase stability issues are recognized and addressed, the introduction of oxalate ($C_2O_4^{2-}$) provides a passivating layer that prevents the leaching of Ba, permits dispersion, and maintains the stoichiometry of the barium titanate.[44] Thus, both recognition of the stable phase(s) in a system and surface chemical approaches to manage the phase stability permit the processing of metastable phases without compromising the ultimate material

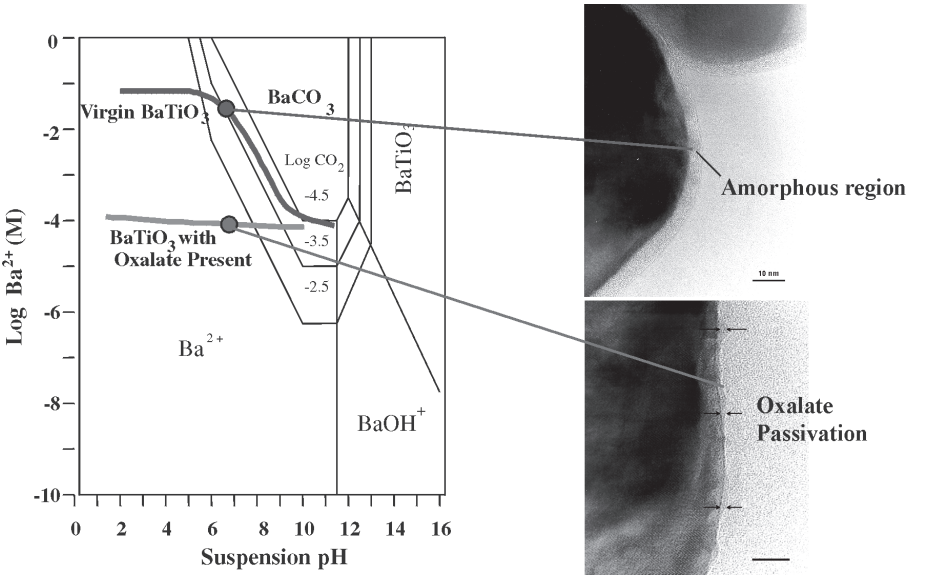

FIGURE 1.2 - Preventing surface defects on nanoscale barium titanate, particles with chemical passivation.

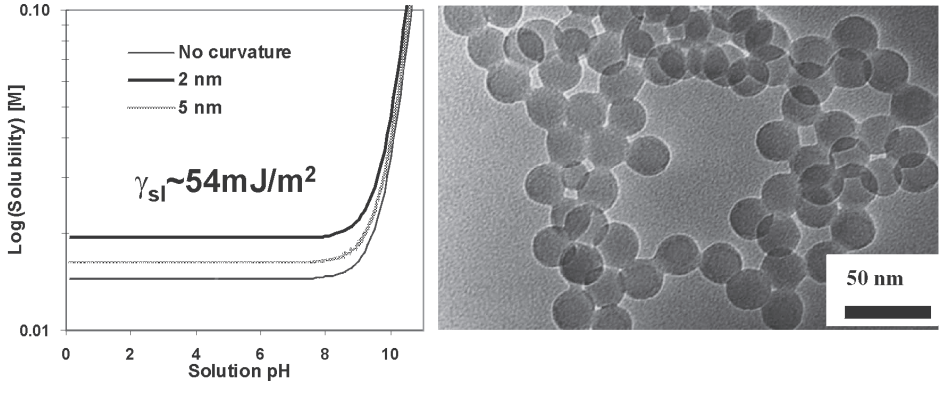

FIGURE 1.3 - Nanoscale effects on solubility (Ostwald-Freundlich, also known as the Thompson-Gibbs Effect) and nanoparticulate aggregation via selective dissolution from smaller particles and deposition at contact points among larger particles.

properties, particularly for nanoscale particulates with a high surface reactivity.

Figure 1.3 gives the solubility of pure, amorphous silica as a function of solution pH and particle size. The solubility curves were calculated using data from Iler[15] and the OPAL program developed in the Particulate Materials Center

at Penn State.* Iler and others have discussed the agglomeration of nanoscale silica as an Ostwald ripening mechanism. However, the TEM photomicrograph in Figure 1.3 indicates that rather than small particles being consumed via the higher solubility shown in the solubility diagram in Figure 1.3, it is more likely that the relatively monosized nanoparticles shown in Figure 1.3 sintered via a liquid phase transport mechanism. Thus, it is more beneficial to protect nanoparticles from liquid mediated sintering, rather than the Ostwald ripening, at least in the silica-water system. This finding is consistent with the notions of protection-dispersion developed by Zsigmondy[2] or passivation-dispersion developed by Adair and co-workers.[41]

1.1.2. Zeta potential and surface charging

There is a relatively large literature on the measurement of surface charge on the nanoscale, but usually not well-dispersed, nanoparticulates.[17-19,24,25,27] All of these techniques are based on potentiometric titrations in which the large surface areas are used to measure the adsorption of H^+(aq) or OH^-(aq) as a function of suspension pH.[17] In general, at least 100 m^2 of powder must be present in the suspension for accurate adsorption measurements, hence, the requirement for large surface area powders. At present there is nothing to suggest that nanoscale particulates have a significantly different pH at which charge changes polarity, the isoelectric point, or that the fundamental charging mechanisms are different from those found with sub-micron and larger size powders.[30] However, as shown in Figure 1.4, the larger surface areas of nanoscale particulates must be accommodated during surface modification. The figure shows the zeta potential as a function of suspension pH for two silica powders, a 300 nm diameter Stöber silica prepared by the hydrolysis of tetraethoxy silane in ammonia, water, and ethanol, and a 20 nm diameter silica prepared by a reverse micelle approach.[45] The zeta potentials for the silica powders are shown for the as-washed silica powders giving good agreement in the isoelectric point for both powders at ~pH 3. In contrast, after treatment with 1 weight percent aminopropyl trimethoxy silane, the low surface area Stöber silica has a saturated surface indicated by the high positive zeta potentials while the high surface area nanosilica is only partially coated with the condensed amine groups with a shift in isoelectric point to ~pH 6. Thus, the high surface areas

** H. Krarup, R.V. Linhart, and J.H. Adair, OPAL - a WindowsTM computer program that calculates the solubility of metal oxides and metal hydroxides as a function of solution pH for both ideal solutions and non-ideal with activity coefficients calculated using Davies' modification to Debye-Huckel's approach. Available by contacting senior author at JAdair@psu.edu*

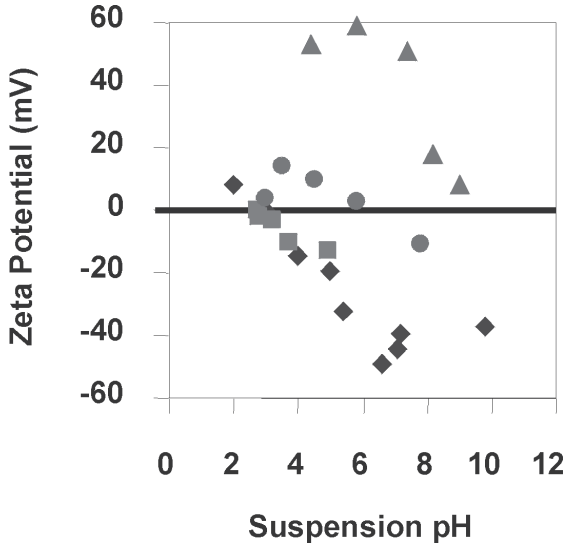

FIGURE 1.4 - Zeta potential of silica macroscopic particulates and nanoscale silica

◆ *Stober silica, as-washed;* ■ *Nano-silica, as-washed;* ▲ *Stober silica with 1 weight percent amino-propyltri-methoxy silane(APS) on the surface;* ● *Nano-silica with 1 weight percent APS condensed on the surface.*

for nanoscale particulates must be recognized and accommodated in processing. This implies that much higher concentrations of dispersants, binders, and other additives used in the processing of conventional powders are required for nanoscale materials. Alternatively, innovative approaches may also be used for surface modification as discussed in the other sections.

1.1.3. Intermolecular forces among nanoscale particulates

The fundamental forces among nanoscale particulates certainly scale with size, but some of the fundamental relationships may also change at the nanoscale.[9,11,13,26,42,43,45] For example, Gatica *et al*[45] have shown that the Axilrod-Teller-Muto 3-body formulation to predict van der Waals interactions among nanoscale particulates is more valid than conventional approaches for macroscopic particulates.[9,11,13,26,42,43] Even if the fundamental forces do not change, there are changes in the Hamaker constant as size diminishes below the intrinsic correlation length, the scale at which quantum effects, particularly those associated with semi-conductor and conductor materials, begin to dominate electronic transitions. Based on optical data on sub-10 nm cadmium sulfide (CdS) taken from Adair *et al*[46], the Hamaker constant was calculated

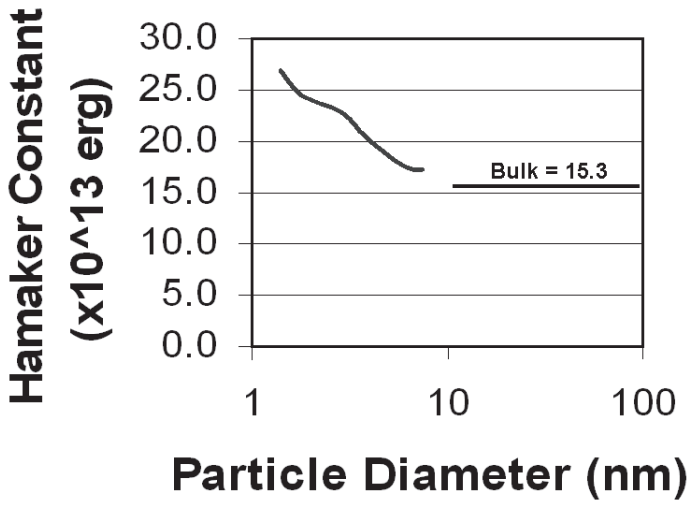

FIGURE 1.5 - Hamaker constant of CdS as a function of size. Based on optical data from Adair et al[46] and the Hamaker constant calculation for semi-conductor materials described by Krupp[12].

for CdS as a function of size. The correlation length for CdS is near 7nm based on the optical data. The Hamaker constant for nanoscale CdS as function of particle size was calculated using the approach provided by Krupp[12] for semi-conductor materials. As shown in Figure 1.5, the Hamaker constant for CdS increases below 10nm particle sizes. This implies that nanoscale CdS is more difficult to disperse with stronger van der Waals attractive forces than the bulk particulates.

The interaction energies associated with nanoscale particulates are also shown in Figure 1.6. The interaction energies were calculated using the STABIL© program developed by the Adair Group.* The Hamaker constants were taken from the values in Figure 1.5. The interaction energy relationships used for the calculation were developed and described by Verwey and Overbeek based on the linear Poisson-Boltzmann relation for the repulsive interactions and the classical van der Waals attractive interactions developed by Hamaker.[7] The ionic strength for the calculations was 10-3M NaCl. As shown in the figure, the repulsive interaction diminishes leading to smaller repulsive energies as particle size diminishes at least based on classical colloidal

** R.V. Linhart and J.H. Adair, **STABIL©**- WindowsTM computer program to calculate the interparticle energies for a variety of solutions. Available by contacting senior author at JAdair@psu.edu*

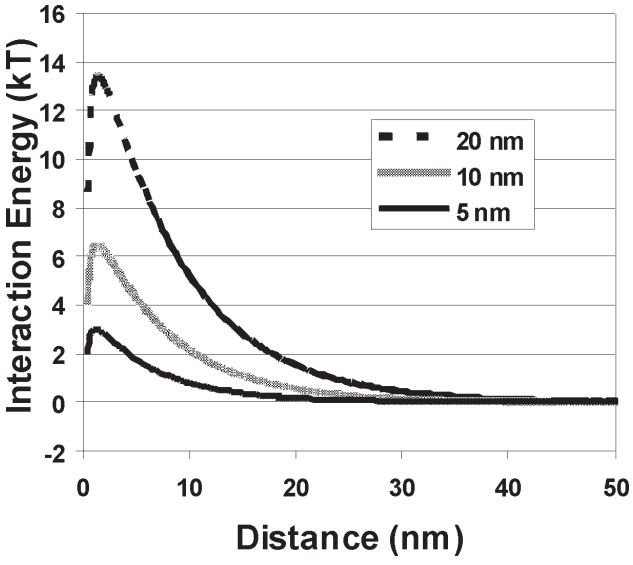

FIGURE 1.6 - Effect of nanoscale particle sizes on interaction energy curves for two particles approaching one another based on the linearized Poission-Boltzmann relationship.[7]

interaction energy theory. However, the curves in Figure 1.6 are not consistent with our experimental findings described below in which robust dispersant schemes have been developed for three nanoscale particulate systems. Therefore, the inconsistencies between theoretical calculations and our experimental observations underscore the need for new theories specifically developed to accommodate the nuances associated with nanoscale colloids such as those developed by Gatica *et al*[45].

1.1.4. Measurements of agglomeration in nanoscale particulates

There are a variety of ways to determine the degree of agglomeration in powders.[17-19,24,25,27] Relative particle size as a function of dispersant concentration, particle sedimentation, rheological evaluations, and packing density are but a few examples. There are two basic approaches to determine the degree of agglomeration in powders that we use, regardless of whether the materials are nanoscale or conventional sizes. The first approach is based on the notion that relatively loose agglomerates are amenable to gas adsorption and the degree of agglomeration does not readily affect the measure of surface area. Comparison of the median volume (V_{50}) by particle size distribution determinations with the average equivalent spherical volume (V_{gas}) calculated from the specific surface area determined by gas adsorption gives the average

agglomeration number. This approach is more thoroughly discussed in Section 2-4.

The second approach is based on particle packing. However, for nanoscale particulates, the size of organic additives can have an impact because of the small particle size. In general, random close packing of spheres gives 64 percent theoretical density or a void volume fraction of 0.36 in a bed of equal sized spherical particles.[36,40] If the particles are coated by a uniform layer of an organic, it can be easily shown that,

$$\textbf{Modified Density} = \frac{\rho_{packing}}{\rho_s}\frac{\left[R^3\rho_s + \left((R+\delta)^3 - R^3\right)\rho_{organic}\right]}{(R+\delta)^3} \qquad [1]$$

where, $r_{packing}$ is the random close packed density, r_s is the density of the solid, $r_{organic}$ is the density of the organic, R is the particle radius, and d is the organic coating thickness. Figure 1.7 summarizes the relationship in Equation 1 showing density as a function of particle size for four different 'organic' coating thicknesses on the particles. As noted in Section 3, the best random close packing that can be achieved with a 10 nm zirconia particle with a 0.37 nm thick oxalate coating is around 53 percent theoretical density. Thus, the role that organic and other materials (e.g., adsorbed H_2O) have on the packing

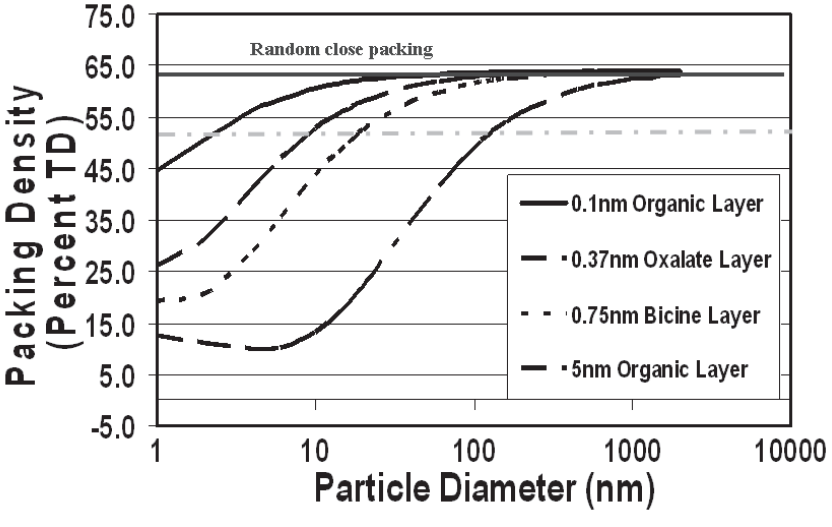

FIGURE 1.7 - Particle packing density as a function of particle diameter and organic layer thickness. The calculations, based on Equation 1 assumes random close packing at 64 percent of theoretical density for idealized hard spheres modified by an organic adsorption layer. Density for the organic layer is assumed to be 1g/cc.

of nanoscale particulates must be recognized and accommodated in evaluating particulate packing behavior.

1.2. Conclusions

The features of nanoscale particulates summarized in Table 1.1 provide a guideline in developing specific dispersant schemes for different nanoscale particulate material systems. Each of these features is incorporated in the three case studies that follow in Sections 2, 3, and 4.

2. DE-AGGREGATION AND DISPERSION OF HIGH CONCENTRATION SLURRIES OF NANOPHASE ALUMINA BY CHEMICALLY AIDED ATTRITION MILLING

Commercialization of nanotechnology through nanoparticle processing is awaiting processes capable of handling and creating aggregate free nanoparticles in bulk quantity[30,47,48]. There are several scientific and technical issues that must be addressed before nanoscale powders are sufficiently developed to be used for bulk material manufacturing. High surface area nanophase powders adsorb significant amounts of water that can affect the reactivity of surface hydroxyl groups[49,50]. Also, drying severity affects the concentration of surface hydroxyl groups, precipitation of surface hydroxyl species and the degree of hydroxylation between the particles[51-53]. Aging of nanophase powders under such conditions were shown to form permanent bridges between that particles, even under ambient conditions[15,54,55]. Bridging leads to neck formation resulting in aggregated particles. The challenge comes in de-aggregating, processing and handling of nanophase powder in high concentration slurries for processing in manufacturing plants[56]. Aggregation is also a critical issue in compaction and densification of starting powder towards successful fabrication of bulk materials and devices[47,47,56,57]. Consolidation of aggregated materials compromises the packing density of green bodies and the final microstructure of the bulk materials[47,58].

Developments on processing of nanophase materials at the Particulate Materials Center, Penn State University, have shown that hard aggregates in nanophase materials can be successfully broken down to near primary particle dimensions by employing a chemically aided attrition milling (CAAM) process. Milling is a dynamic process that involves concurrent events including breakage of particles, breakage of aggregates and agglomeration. The resulting particle sizes obtained via milling are controlled by the material and aggregate properties, available breakage mechanisms, and the energy or power input during milling[59-61]. Chemically aided attrition milling (CAAM) parameters were optimized for de-aggregating nanophase alumina powder by Kumar *et al*[62].

The results summarized here are on CAAM of nanophase alumina particles, de-aggregated from a median size of 11 nm to a median size of 20 nm in 1 hr of milling.

2.1. Materials and methods

Ultra fine milling/de-aggregation of ceramic particles by the CAAM process has been reviewed by Mandanas *et al*[44]. The mechanism of de-aggregation in the CAAM process is similar to that of "stress corrosion cracking," shown in Figure 2.1a. Experimental and theoretical studies have shown that reactive species (e.g. water, ammonia, etc.) can attack at strained bonds in pre-existing surface flaws. Preferential dissolution at the highly strained crack tips promotes crack growth to a critical flaw size, at which point unstable and rapid crack propagation causes the material to fail[63-65]. In CAAM, similar behavior is expected to take place at strained bridges between the aggregated

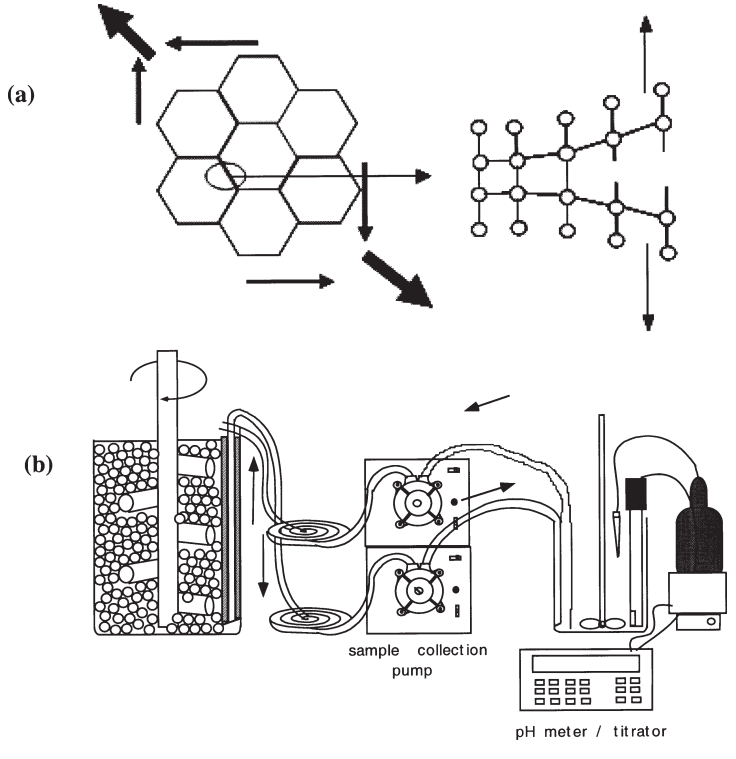

Figure 2.1 - Schematic of: (a) "Stress Corrosion Cracking," the mechanism of de-aggregation in CAAM process. The reactive species, e.g. water, ammonia, etc. attack at strained bridges between the aggregated particles, promoting de-aggregation under suitable chemomechanical environment. (b) Experimental setup for pH stat milling experiments[23].

particles, promoting de-aggregation in suitable chemomechanical environments. Therefore, solvent chemistry (e.g., suspension pH) during CAAM should be selected such that the material being milled has some degree (10 percent to 100 percent) of elevated solubility in the solvent. The schematic of the experimental setup for the CAAM process is shown in Figure 2.1b[66]. The suspension is continuously circulated and titration performed to maintain suspension pH in a dynamic and continuous manner during milling.

CAAM was performed on nanophase Al_2O_3 (mixed phases of γ-Al_2O_3 + δ-Al_2O_3) powder, provided by Grace Davison Catalysis, Columbia, Maryland. The powder had a specific surface area of 116 m^2/gm, as measured by the Brunauer-Emmett-Teller (BET) gas adsorption technique, with an equivalent spherical diameter of 16 nm[55]. The as-received powder had a median aggregate size of 11 μm as measured by a light scattering technique (Malvern Zetasizer*). Details on the experimental process for CAAM of nanophase alumina have been given previously[62]. A suspension with 25 vol% (50 wt %) alumina powder was milled with 0.2 mm high purity ZrO_2 (Y_2O_3 stabilized) milling media, at an agitator shaft speed of 2000 rpm and powder addition rate of 2.0 gm/min. Selection of milling parameters were based on optimized guidelines suggested by Kumar *et al*[62].

Suspension pH was selected to provide the slightly elevated solubility of alumina to promote dissolution at crack tips for stress corrosion cracking. The solubility-pH diagram or "Predominance Area Diagram" for alumina is shown in Figure 2.2[67]. The shaded region in the diagram, showing elevated solubility with decreasing pH, was explored for de-aggregation by the CAAM process. Optimum pH was set to pH 4.0 ± 0.25 by an elimination method based on preliminary experiments. Suspension pH values either lower or higher did not provide dispersion or the elevated solubility required for CAAM. Suspension pH drifted towards the basic side as milling proceeded. Concentrated hydrochloric (HCl) acid was used as a reagent to dynamically readjust the pH and limit pH drift within pH 3.75-4.25 during the milling process using the titration system.

Small amounts of suspension were extracted at 10, 20, 40 60 and 120 min during milling, to measure the milled, sub-micron particle size distributions using a quasi-elastic light scattering system (Malvern Zetasizer*), and suspension viscosity using a plate-cone arrangement on a CSL Rheometer**. The effect of milling was also observed by comparing SEM*** and TEM****.

** Malvern Instruments Ltd. Malvern, UK*
*** TA Instruments Ltd., New Castle, DE*
**** Hitachi S-3500N SEM, Hitachi Instruments Inc., Japan*
***** JEOL 2010F high-resolution-TEM, Japanese Electronics and Optics Lab., Japan*

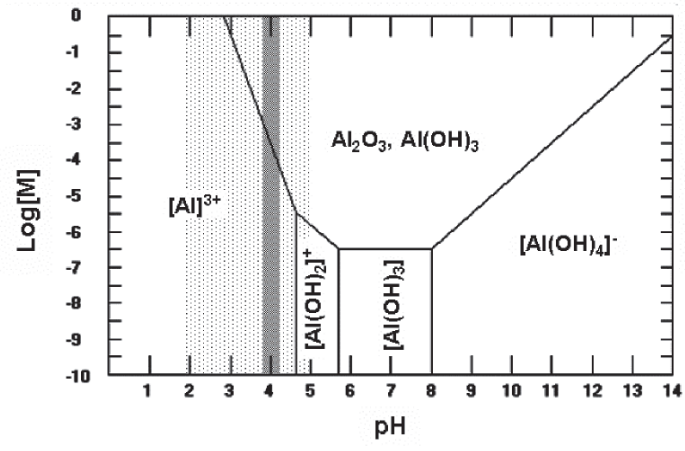

FIGURE 2.2 - Theoretical solubility vs. pH plot (Predominance Area Diagram) of alumina. Thermodynamic data taken from Baes & Mesmer[67]. The shaded region in the diagram, showing elevated solubility with decreasing pH, was explored for de-aggregation by CAAM process. Optimum milling pH was set to pH 4.0±0.25[62].

micrographs obtained on selected samples before and after milling. The states of dispersion of the milled suspensions were estimated by calculating the average agglomeration number (AAN). As noted in Section 1, the AAN gives an approximate estimation of the number of primary particles in an agglomerate/aggregate. An AAN of 10 or less is considered to be a well dispersed suspension suitable for additional processing. AAN is calculated by taking the ratio of the volume of the agglomerate/aggregate to the volume of the primary particle[68].

2.2. Results and discussions

Performance of CAAM on nanophase alumina powder was recorded as average agglomeration number *(AAN)* and suspension viscosity after milling for 10, 20, 40 60 and 120 min, as shown in Figure 2.3a. De-aggregation below an *AAN* value of 10 could be achieved in less than 1 hr of milling. Figure 2.3b compares the particle size distributions for the nanophase alumina before (as-received powder) and after milling. The milled suspension particle size distribution has two peaks, a major peak at ~30 nm and a minor peak (composed of about 10 vol % of the total distribution) at ~250 nm. The effect of CAAM on aggregate size was verified by SEM and TEM micrographs on samples collected before and after milling that are shown in Figure 2.4. The SEM micrograph of as-received alumina powder corresponds to the median particle size of 11 μm. The TEM micrographs obtained after milling for 1 hr

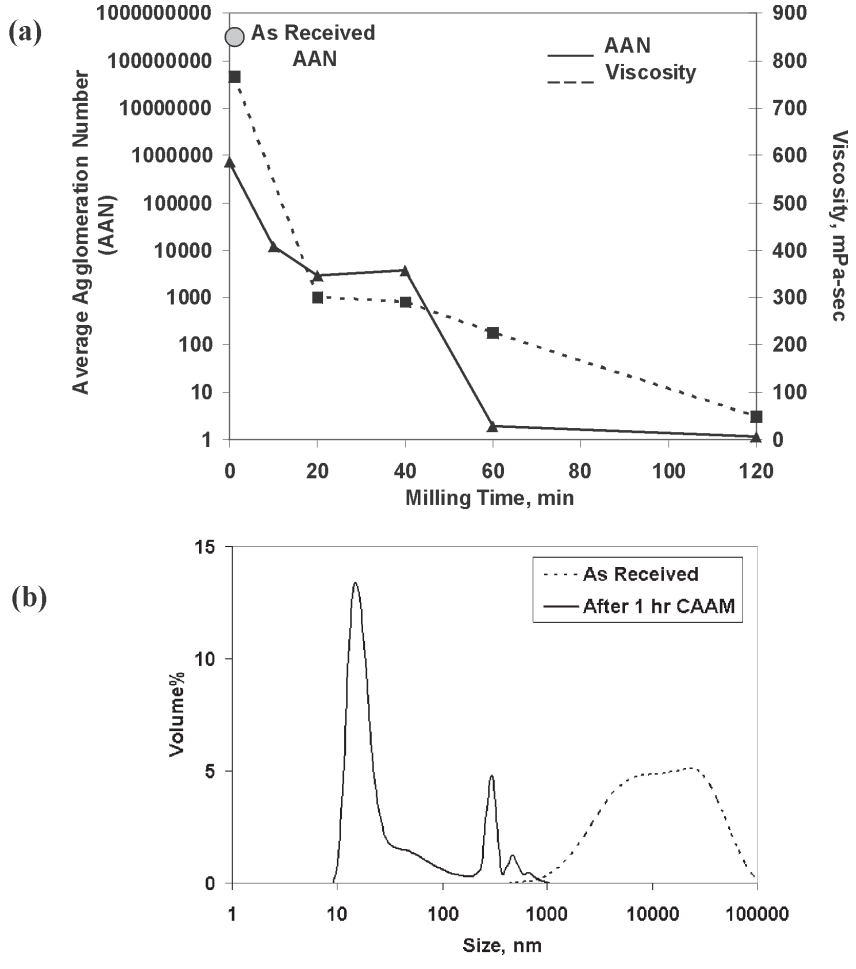

FIGURE 2.3 - (a) Change in Average Agglomeration Number (AAN) and suspension viscosity with milling time (Suspension pH 4.0±0.25; Concentration 25 vol% (50 wt%)). (b) Particle size distribution for as-received aggregated nanophase alumina (AAN ~300,000,000); and suspension obtained after CAAM at pH 4.0±0.25 for 1 hr (AAN ~10)[62].

show dispersed alumina nanoparticles in clusters of 5-15 primary particles with sizes between 20-50 nm, and a few larger clusters about 250 nm in size.

The design of experiment studies performed on CAAM of alumina have shown that using small media is critical in milling below an ANN of 10[62]. The use of small media distributes the same amount of power or energy input for the milling into an increased number of positive de-aggregation mechanisms

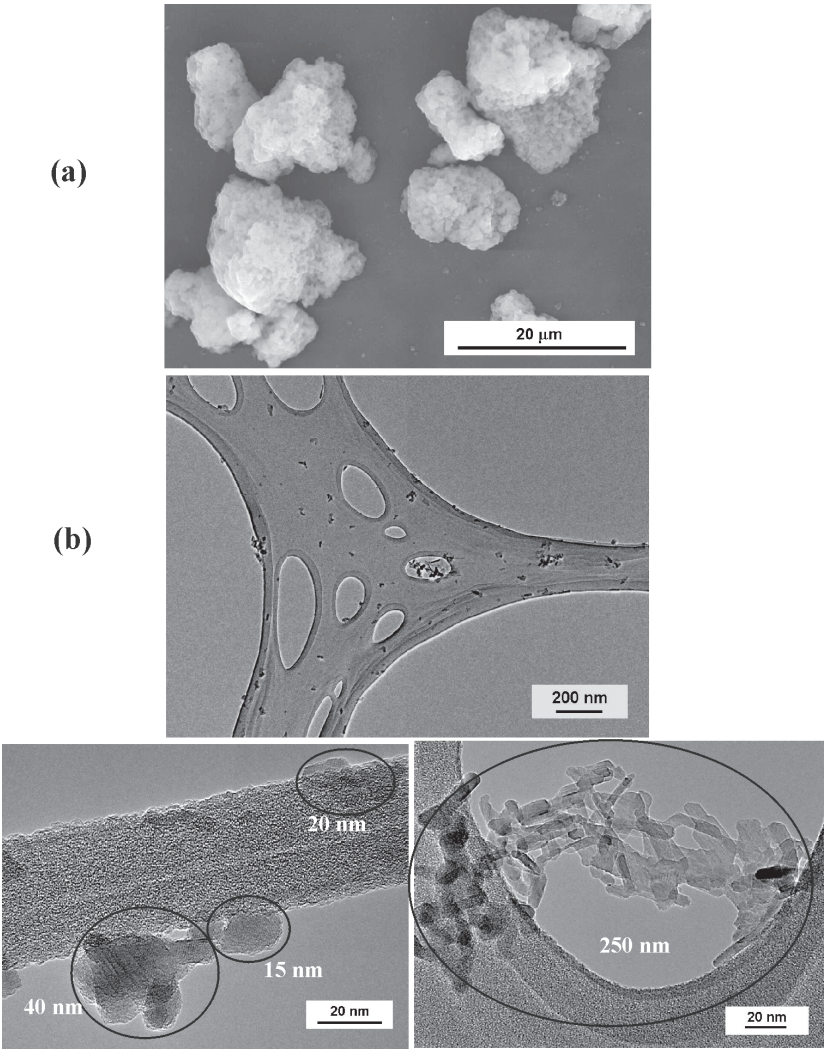

FIGURE 2.4 - (a) SEM micrograph of as-received nanophase alumina (before milling) with AAN ~300,000,000. (b) TEM micrographs for chemically aided, attrition milled nanophase alumina with AAN ~10. Sample collected after 1 hrs of milling at pH 4.0±0.25. About 10 vol% of suspension has ~250 nm aggregates, also seen in TEM micrographs[62].

including collision, abrasion and shear, resulting in breakage of the aggregates We believe that the finer media has enough mass to generate momentum that can exceed the minimum stress required by the aggregate to create a positive de-aggregation event[61]. The small particle sizes observed in the samples after CAAM support this assertion.

The suspension viscosity decreased from about 800 mPa-sec to 50 mPa-sec with milling time as shown in Figure 2.3a. Decreases in suspension viscosity with milling is due to release of trapped water within the open pores inside the aggregates. The trapped water in the interpore spaces of the aggregates effectively increases the solid content in the suspension with less water available to support shear in the aggregated suspensions. As milling proceeds, the trapped pore concentration reduces with reduction in aggregate size, releasing the trapped water and providing additional dispersing medium resulting in lower viscosities.

2.3. Conclusions

Chemically aided attrition milling (CAAM) has shown potential to de-aggregate and disperse aggregated nanophase materials to near primary particle dimensions. The critical parameters to consider are (1) control of suspension chemistry (e.g. suspension pH) to achieve an elevated solubility of aggregate material to promote stress corrosion cracking at the aggregate bridges/necks; and (2) use of smaller media to increase collision, abrasion and shear events for more efficient use of input energy. Future work will focus on optimizing material specific suspension chemistry and milling parameters to achieve de-aggregation to primary particles in minimum time and media wear. We also intend to develop processing for bulk nanograin materials from the de-aggregated nanoscale particulates.

3. NANO-ZIRCONIA SYNTHESIS AND PROCESSING

There are a variety of ways to produce nanosized Y-stabilized zirconia powder, including, but not limited to, polymerization/sol-gel, coprecipitation, and hydrothermal methods.[70-87] In some instances, precipitation reactions occur out of a homogeneous solution.[77,80,88,89] This method of precipitation takes advantage of nucleation/ growth concepts to produce ultra-fine particles. Using complexation chemistry, the participating metal ions are kept in a dissolved state to produce a homogeneous solution. Precipitation takes place when the complex is broken and large amounts of metal ions are dumped into solution. When the metal-ligand complex is broken, the supersaturation of the solution is extremely high, and almost all the energy available for growth is consumed in the formation of nuclei. As a consequence, little growth of the nuclei occurs and the resulting particles are ultra-fine in size.

The choice of complexing agent is based on several considerations. First, the complexing agent needs to form a stable complex with the metal ions over a wide range of pH values. Second, the complexing agent should impart charge to the surface of the precipitated particles to promote dispersion

in suspension. Furthermore, a complexing agent with simple chemistry is desirable for ease in solution preparation and for subsequent processing steps. Complexing agents have been studied in detail for many years,[90-94] specifically including several for zirconium in aqueous solution.[90-92] The complexing agents identified in these studies[90-92] were based on multidentate ligands. The goal of the present study was to find stable chelating compounds for zirconium ionic species that operate over a wide range of pH values. Furthermore, for the processing of nanoparticles, there is a critical need for a complex with dispersive capabilities to keep the synthesized nanoparticles from aggregating in suspension during subsequent laundering and collection steps.

The complexing agent was chosen to serve two purposes: first, to chelate Zr and Y ions, keeping them in solution up to a pH value of 13; second, to prevent nucleated particles from aggregating by means of an electrostatic dispersion mechanism. Bicine was identified as a suitable complexing agent because it met these needs.

In aqueous solution, it is known that dissolved zirconium will create a drift in pH to values around or below 1 because of the formation of zirconyl hydroxide complexes. Solubility data suggests that zirconium hydroxides will begin to precipitate as the solution pH approaches values from pH 1.5 to pH2.[67] The addition of a yttrium dopant compound tends to raise the solution pH above these critical values, which can lead to premature precipitation. Thus, the complexing agent must be present before the dopant is added to the Zr ion solution. Once the complexing agent is in place, Y-ion stock solution can be added and the solution pH adjusted to the desired alkaline pH value. Precipitation at alkaline pH values is preferred with respect to the solubilities of Y and Zr and the desire to precipitate the tetragonal phase.[79,95] Once the homogeneous solution has been prepared, a hydrothermal treatment can be used to break the complex and cause instantaneous precipitation of nuclei with little or no growth (see Figure 3.1). The precipitated particles are 6-10 nm in size and tetragonal in phase (see Figure 3.2).

3.1. Washing and recovery

In the aqueous processing of nanoparticles, the concept of a protective colloid can be used in the recovery and dispersion of nominally 8 nm 1.7 Y-TZP particles. In previous studies, it was found that as-synthesized agglomerates were dispersible by ultrasonication.[96] It was also determined that bicine (see Figure 3.3) acts to reversibly agglomerate the as-synthesized particles. In order to remove the flocculant, bicine, from the surface of the particles, a procedure for washing was developed in which the particles were centrifuged and then redispersed in a non-flocculating solution. During the centrifugation, the bicine surface layer acts as a protective shell preventing particle on particle

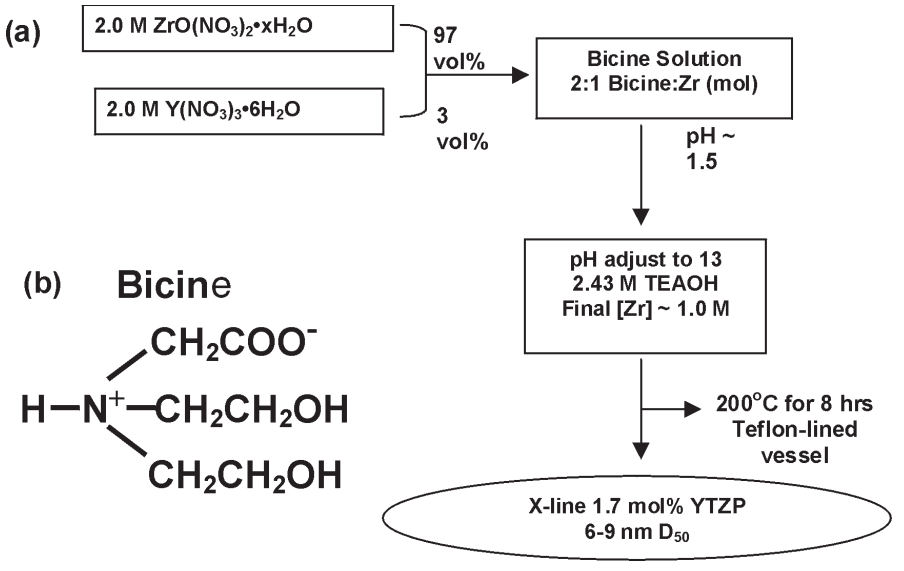

FIGURE 3.1 - (a) Flowsheet describing the procedure for the synthesis of 6-10 nm zirconia and yttria-stabilized zirconia.[108,118,119] (b) Bicine is used as a complexing agent to keep zirconium and yttrium ions in solution. During hydrothermal treatment, the metal-bicine complex is broken and nuclei are dumped into solution with little or no growth.

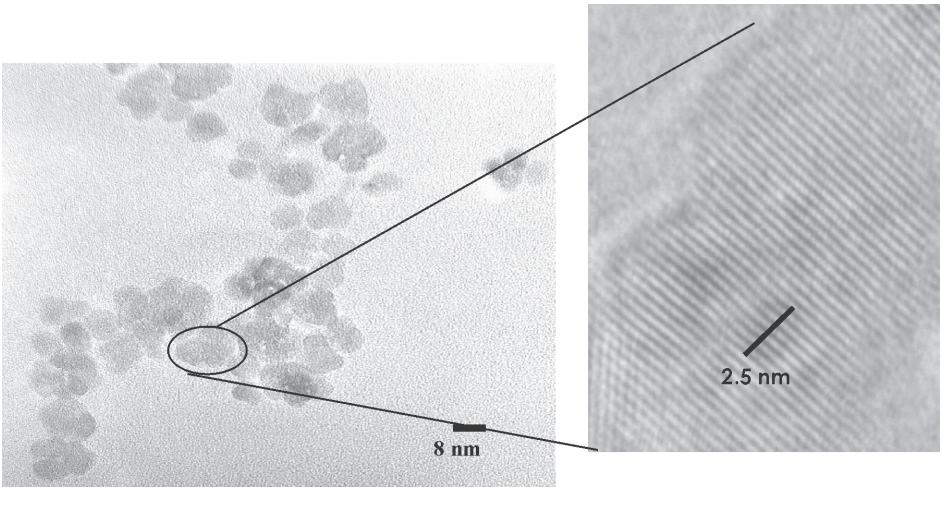

FIGURE 3.2 - High resolution TEM photomicrograph shows individual zirconia particles to be 6-10 nm in diameter.

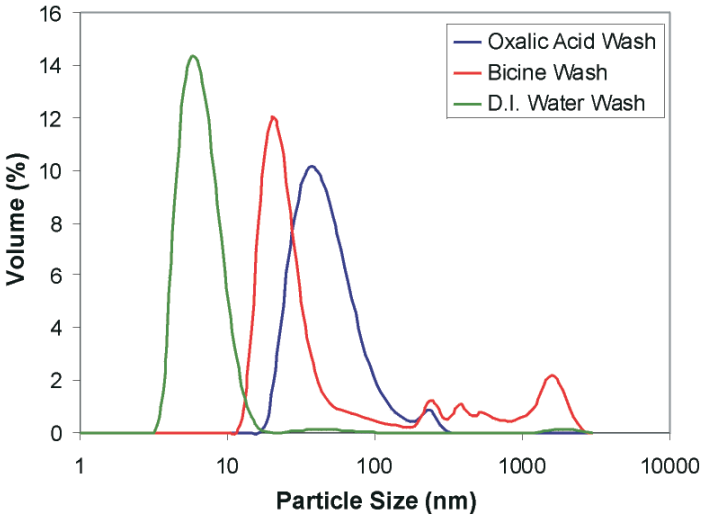

FIGURE 3.3 - Particle size distribution of aqueous zirconia suspensions measured by quasi-elastic light scattering for different wash treatments. Washing with oxalic acid reduces agglomeration caused by the presence of bicine and provides stable dispersion.[96] When suspensions are washed with deionized water, reversible agglomeration and dispersion is achieved through the presence of residual bicine adsorbed to particle surfaces.[120]

contact. Furthermore, it was hypothesized that bicine acts in the classical sense of an association colloid, which is reversibly associated with the Y-TZP particles, such that it could be removed by washing. By taking advantage of the reversible nature of bicine, a more effective dispersant could replace bicine on the surface of the particles and allow for the creation of a stable, well-dispersed 1.7 Y-TZP suspension.

Oxalate (see Figure 3.3) was chosen as the final dispersing solution based on its efficacy as a surface passivation agent and ability to impart reasonable quantities of negative charge on zirconia particle surfaces.[97] From a previous study on the aqueous degradation and surface passivation of 3 Y-TZP, oxalic acid was found to provide significant surface charge which permits the recovery based on the concept of protection-dispersion.[97] In addition to the surface charge provided, an increase in zirconium concentration was observed in solution with the addition of oxalic acid. It was proposed that by washing the powder in an oxalic acid solution of controlled solution pH, the bicine could be displaced by increasing the solubility of the zirconium to which bicine is complexed. Once the surface layer is removed, oxalate is free to form an adsorbed, passivation layer on the exposed zirconium surfaces.

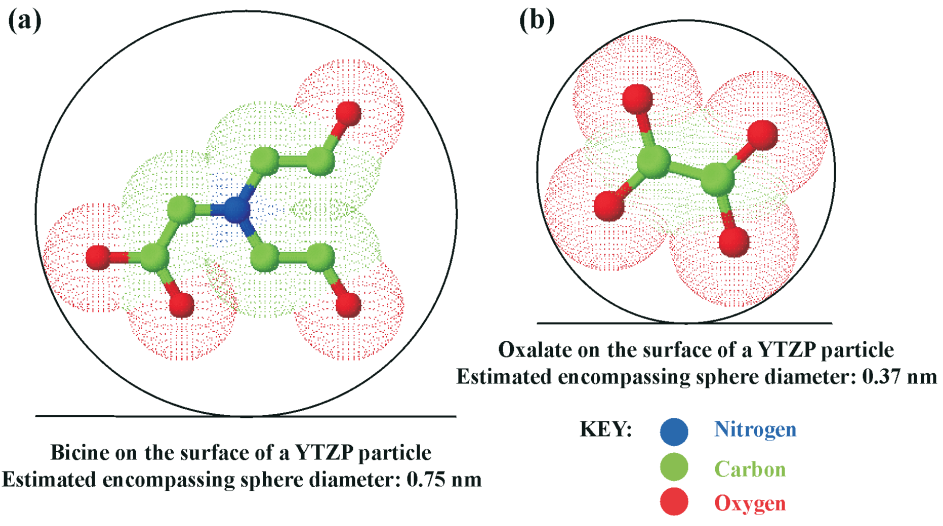

FIGURE 3.4 - Space-filling models of (a) bicine and (b) oxalate ions allow an estimation of each molecule's approximate spherical diameter.[121]

The effectiveness of several other wash solutions on zirconia dispersion has also been evaluated in subsequent studies (see Figure 3.4). Since bicine is already present in abundance in the precipitate suspension and has been observed to prevent permanent particle aggregation, it was hypothesized that it may also act as a dispersant once the majority of the reaction by-products were removed. It was also believed that, as long as the bicine surface layer was not removed from precipitated particles, spontaneous dispersion could be achieved in an aqueous medium once reaction by-products and the ionic strength (i.e., total ions present) were removed or at least largely reduced. In each of these cases, stable dispersions of primary particles were achieved within 5-8 wash cycles.

3.2. Solid body formation

Previous studies have demonstrated that wet processing routes provide the best route to obtain bulk, nanocrystalline ceramics because wet processing permits maintaining a well-dispersed state to promote particle packing. In contrast, developing the soft agglomerates required for powder pressing operations, while part of our longer term strategy to produce bulk materials, is a longer term prospect in which only preliminary studies have begun.[98-100] A majority of ceramic components made from powders with sub-micron powders are generally formed using dry pressing techniques such as uniaxial or isostatic compression. However, use of these techniques with nanosized

powders is inherently difficult due to consolidation and energy issues.[98,101-105] Nanosized powders are significantly affected by hydration forces which can lead to aggregation in suspension. This in turn can lead to the problems of poor powder flow and poor packing of the powder particles in the die. The high surface area associated with nanosized powders can lead to friction problems along the die wall also giving poor flow and powder packing. These problems also contribute to the need for forces larger than the capabilities of most conventional presses and greatly inhibit the ability to make large bulk samples given the present state of the art.

Wet processing techniques avoid the problems of dry forming techniques by keeping the powder in a suspension. Using a well-dispersed suspension circumvents the issues of powder flow and powder packing, leaving only the problem of consolidation to overcome. Consolidation during wet processing can be addressed by drying techniques and/or the application of a load.

Drying bodies without application of a load is a technique used in evaporation, sol-gel drying and slip casting. Evaporation has problems for nanoparticulate bodies due to agglomeration and phase separation while driving off solvent with the application of heat.[104,105] Evaporation without stringent control of heating can also lead to the development of drying stresses in the body. Drying defects produce internal defects and cracking, which are catastrophic in the formation of a solid body by sintering. Sol-gel drying is similar to evaporation drying in producing drying stresses due to the large amount of solvent that has to be removed from fine pores for consolidation.[106] As a consequence, sol-gel drying is typically only applied to bodies that are thin and/or with small dimensions.

Slip casting is performed by placing a suspension into a porous mold which removes solvent via capillarity forces in the finer pore structure of the mold.[36, 40] However, suspensions of well-dispersed nanosized particles will have nanosized pore with capillary forces much greater than those found in a typical mold material. Thus, there will be no driving force for consolidation of the nanosize particle body and, as a result, poor consolidation and low green densities will be obtained. Forces in addition to the capillary forces must be applied for the green forming of nanocolloids.

Wet processing techniques that use the application of hydraulic or mechanical forces for consolidation include centrifugation and filter pressing. Centrifugation uses centrifugal forces to pack powder particles by accelerated sedimentation. Sub-micron alumina powders have been consolidated in this manner; also, centrifugation has been used for recovery of the well-dispersed as-synthesized Y-TZP powder.[106] However, a wide particle size distribution can lead to mass separation in the final compact. And, conventionally, centrifuge

tubes are limited in size and shape.

Filter pressing[104,105,109-114] consolidates suspended powder by pressing the suspension into the bottom of a die placed over a porous membrane. The membrane allows the supernatant to pass through, leaving behind a consolidated powder compact. Since the powder is in suspension, friction between the die walls and the powder is minimized and, as such, much lower pressures are required for compaction compared to dry pressing. However, there is little information on the drying and sintering of as-pressed pellets from nanoscale particulates. Furthermore, cracking issues associated with drying filter pressed pellets have not been satisfactorily addressed. Despite the lack of literature and the drying issues, filter pressing provides an excellent opportunity to form bulk bodies from nanosized particles.[107] Transparent pellets

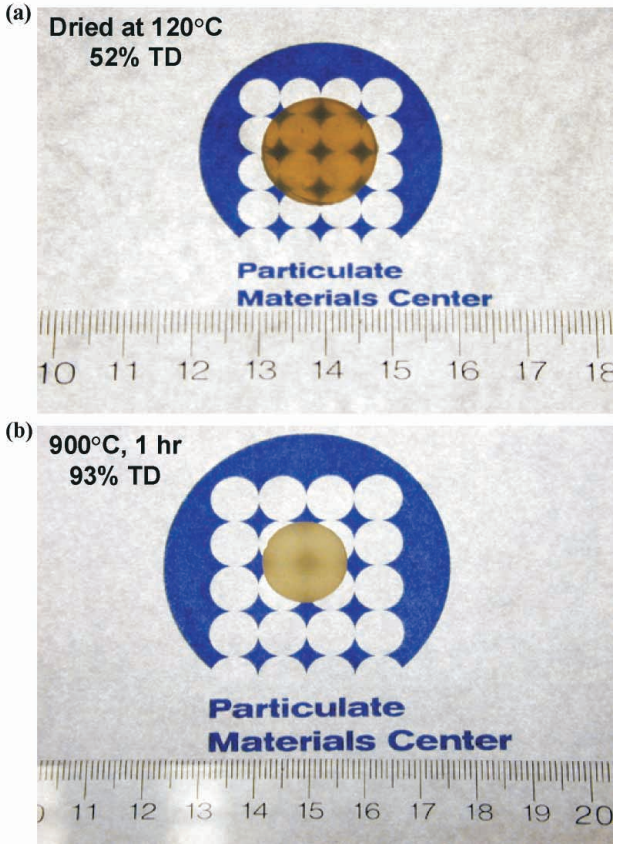

FIGURE 3.5 - (a) Green bodies are formed by filter pressing well-disperse nano-zirconia suspensions and drying at 120 °C under carefully controlled humidity. (b) Filter-pressed pellets can then be sintered to high density.

of 1.7Y-TZP with a nominal thickness of 2-3 millimeters and density of 48% of theoretical were produced by filter pressing by Kimel *et al*[108] (see Figure 3.5).

Once homogeneous, nano-grain green bodies are recovered, sintering techniques can be applied which maximize densification while minimizing grain growth. Transient sintering,[115-117] first described by Chen *et al*, takes advantage of the activation energy difference between grain boundary migration and grain boundary diffusion. Chen *et al* described this sintering approach as densification in a frozen microstructure.[116,117] By first heating rapidly to an elevated temperature, both mechanisms are active, providing densification to a point where pores become unstable against shrinkage. After this density (around 70%TD) is reached, the body is rapidly cooled to a temperature 100-400 °C lower than the initial temperature and held for a prolonged period. This second step allows densification by grain boundary diffusion while limiting grain growth by grain boundary migration, the higher activation energy process. In this work, filter-pressed zirconia bodies composed

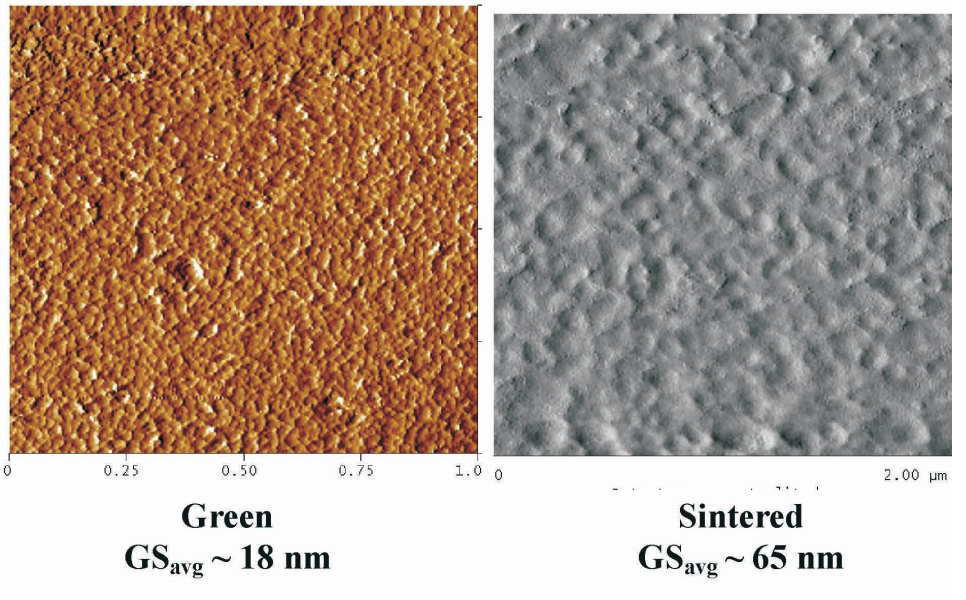

FIGURE 3.6 - Tapping mode AFM images of (a) a dried, filter pressed green pellet and (b) a transient-sintered body show how the nano-scale microstructure is preserved with the two-step transient sintering technique.[115-117] The first step allows pores to reduce to sizes blow which they are unstable against shrinkage; the second, lower temperature step promotes grain boundary diffusion while suppressing grain boundary migration, which maximizes densification and minimizes grain growth.

of 6-10 nm primary particles have been sintered to full density with grain sizes between 60-100 nm (see Figure 3.6).

3.3. Conclusions

A goal of aqueous processing of nanosized Y-TZP powders is the production of bulk Y-TZP ceramics. In order to accomplish this goal, several issues have been addressed. First is the synthesis of nano-crystalline Y-stabilized zirconia, which is achieved by hydrothermal precipitation. The use of bicine as a complexing agent provides a measure of control over particle nucleation while creating a protective barrier against irreversible agglomeration in suspension. Upon the production of nanosized Y-TZP, recovery and dispersion of the powder must take place through a displacement washing procedure. Once this is accomplished, wet processing techniques, which take advantage of the well-dispersed nature of particles in suspension, can be used to consolidate the nanosized Y-TZP powder into a bulk Y-TZP ceramic body. With a sintering technique that maximizes densification while minimizing grain growth through kinetic factors, dense, nano-grain, transparent Y-TZP bodies can be produced. The effect of nano-scale microstructure on mechanical properties will be the subject of future research.

4. SYNTHESIS OF NANOCOMPOSITE COLLOIDS FOR NANO-MEDICAL APPLICATIONS

The active medical agent (AMA) nanocomposite particles possess several qualities that make them attractive for biomedical applications including bioimaging, drug delivery, and gene therapy. The organic fluorescent nanoparticles can be used for bioimaging to monitor the movement of labeled cells in cultures, tissues or intact organisms because the fluorescent emissions from the nanoparticulates are not intermittent unlike the semi-conductor-based fluorescent quantum dots. The nanocomposite particles containing therapeutic agents applied to drug delivery systems permit the utilization of numerous water-insoluble and unstable drugs. The AMA nanoparticles can also be utilized in active drug targeting and extended release applications based on the resorbable shell-matrix.[122] The nanocomposite particulates also have the potential to be used in gene therapy for the delivery of therapeutic DNA to cells.[122] Furthermore, the AMA composite particle sizes (5 – 20 nm) are compatible for biological applications.[123,124] Furthermore, the fluorescent molecules can be combined with the drug or gene therapeutic agents for multifunctional particles capable of simultaneous bioimaging and therapeutic agent delivery.

The use of nanoparticles in biomedical applications is a major focus of

numerous research groups today.[125-127] Roy *et al* reported that current AMA "carriers" include micelles, liposomes, low-density lipoproteins, polymeric micelles, and hydrophilic drug-polymer complexes.[128] Moghimi *et al* reported on drug delivery via nanoparticles such as polymeric nanospheres, ceramic nanoparticles, polymeric micelles, dendrimers and liposomes.[129] Sahoo and Labhasetwar also reported on current nanoparticles used in bioimaging such as magnetic nanoparticles, ferrofluids and quantum dot technologies.[127] Davis reported that three main types of gene therapy have been studied including viral vectors, non-viral vectors and the direct injection of genetic material into tissues.[130]

Major problems in the various schemes for generating nanoparticles for various applications including nanomedical is the poor colloid stability in nanoparticle suspensions including agglomeration, polydispersity in size and shape, swelling and leakage.[128,131] Other limitations include difficulty of synthesis and processing techniques, inadequate drug loading inside the carrier particle and lack of applicability to a variety of medical agents.[132] Residual precursor materials present in unwashed nanosuspensions can also have detrimental effects for both delivery and toxic effects on the physiological system.[133]

Methods for the synthesis of stable, unagglomerated nanoparticles for nanomedical applications in a range of sizes have been developed based on reverse micelle techniques in the current work. The nanocomposite particles can include numerous medically active substances such as organic fluorophores, therapeutic agents and cDNA encapsulated within the nanoporous struncture of silica, titania, calcium phosphate or calcium phospho-silicate nanoparticulate matrices. The nanocomposite particulates are tailored to specific biomedical application based on the selection of core and shell materials.

4.1. Silica NanoComposite particles

The synthesis of SiO_2 matrix nanocomposite particles was performed using reverse micelle techniques followed by the hydrolysis and condensation of precursor materials in the microemulsion matrices.[123] Figure 4.1 illustrates the nanocomposite particle synthesis approach using reverse micelle techniques.[134-136]

The synthesis of silica nanoparticles has been extensively reported in literature. This method used to prepare the spherical SiO_2 nanocomposite particles is based on methods outlined in detail by Adair *et al* and Li *et al*.[134,135] A variety of research has been published on the synthesis of fluorescent silica nanoparticles based on Li's technique.[137-142] To perform the nanocomposite particle synthesis, nonionic surfactant, polyoxyethylene(5)nonphenyl ether

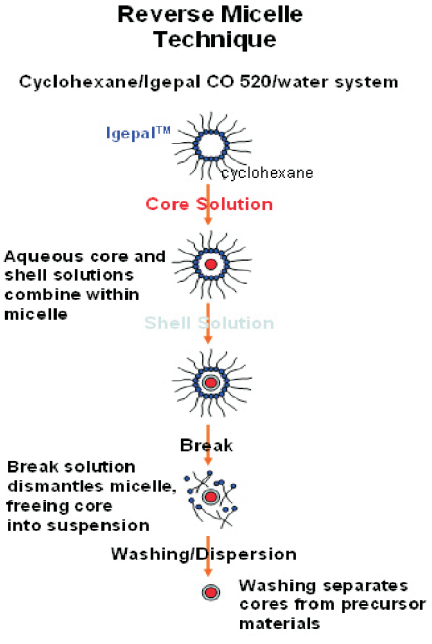

FIGURE 4.1 - Schematic of the reverse micelle synthesis process.

(Igepal® CO-520), cyclohexane, tetraethoxysilane (TEOS), 3-aminopropyltrimethoxysilane (APS), and NH_4OH (28-30%) were obtained from Aldrich Chemical Co. (Milwaukee, WI). Dehydrated ethanol (200 proof, Pharmca Products Inc. Brookfield, CT) was also used. All chemicals in the synthesis were used as received. All aqueous stock solutions were prepared with deionized water (specific conductivity = 0.4×10^{-7} S/m).

Figure 4.2 outlines the synthesis of the AMA/SiO_2 nanocomposite particles. To form the reverse microemulsion, 4 mL Igepal® CO-520, 10 mL cyclohexane and a specific volume of aqueous solution containing an active medical agent are combined by stirring at moderate speed for approximately 30 minutes, resulting in a uniform mixture. The NH_4OH is then added and the suspension stirred for 15 minutes, followed by the addition of TEOS. Full maturity of the micelles occurs roughly 24 hours after TEOS addition. After the 24 hours, a silane coupling agent in the form of APS is added to the suspension to modify the surface charge of the particles.[10,22-24] The microemulsion is broken while rapidly stirring with 50 mL of 0.02 M acetic acid/ethanol solution to maintain a pH value less than pH 7.0.

The size of the nanocomposite particles can be modified through the manipulation of processing parameters including the ratio of water to surfactant

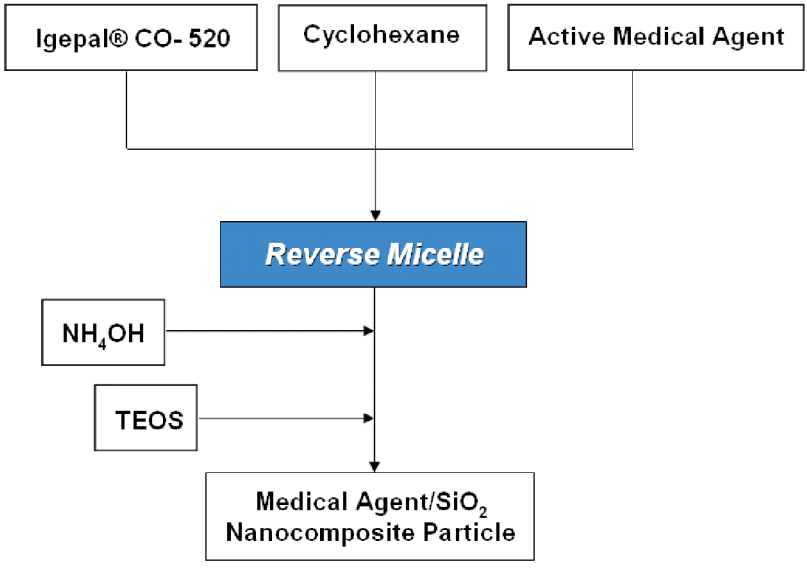

FIGURE 4.2 - Synthesis flowchart for active medical agent/SiO_2 nanocomposite particles.[135]

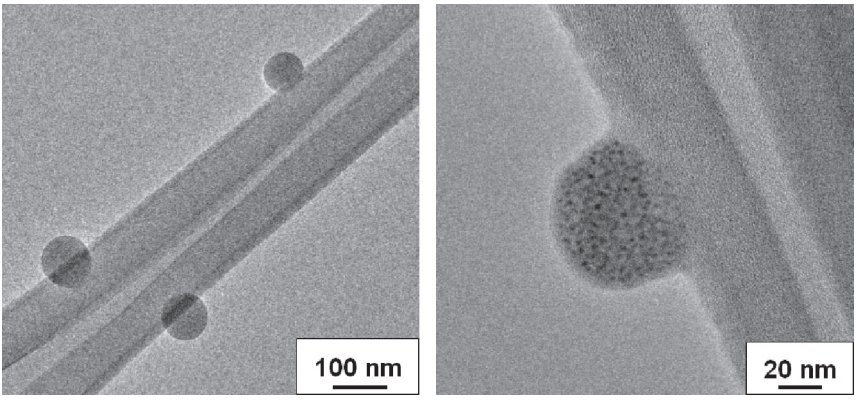

FIGURE 4.3 - TEM images of cascade blue acetyl azide/SiO_2 nanoparticles. (TEM photomicrograph courtesy of J.A. Nelson).

and the ratio of water to precursor materials.[135,136] A spherical SiO_2 nanocomposite particle of approximately 10 nm can be synthesized when R=[water]/[surfactant]=2, H=[water]/[TEOS]=100, and X=[NH_4OH]/[TEOS]=1 is applied to the cyclohexane/water/ Igepal® CO-520 system. The small size achieved allows for evasion of capture by the reticuloendothelial

system (RES) of animal models or the human body, permitting the nanoparticles to function in biological systems by crossing physiological membranes such as the intestinal wall and the blood-brain barrier.[127,145,146]

The SiO_2 polymerization and TEOS hydrolysis rates are slower in a microemulsion synthesis environment than in an aqueous solution.[147-149] The resulting monosize nanocomposite particles for bioimaging consist of organic fluorophore molecules doped throughout the silica nanoporous network. Figure 4.3 illustrates the ultra-structure of ~60 nm cascade blue acetyl azide/ SiO_2 nanocomposite particles. The ease of particle size tunability permits relatively large nanoparticles to be examined that are more easily observed for the dye molecules distributed throughout the SiO_2 matrix.

4.2. Washing and dispersion of NanoComposite particles

The primary challenge in the removal of indifferent species after synthesis is that washing involves the removal of residual precursor materials and excess active medical agents while maintaining nanoparticle dispersion. Washed particles are more easily and accurately characterized due to the absence of residual organics interfering with techniques such as transmission electron microscopy (TEM) and quasi-elastic light scattering (QELS). It is also important to remove co-ions such as nitrate, acetate, and sodium to establish reliable processing for surface Functionalization. Washing nanoparticles for biological applications is a critical step since surfactants and other organic materials have detrimental toxicological effects.[128,133]

The dispersion scheme involves the application of protection-dispersion theory to the AMA nanocomposite suspensions.[2,150] Dispersion of the AMA nanocomposite particles is further enhanced by the use of size-exclusion high performance liquid chromatography (HPLC) to simultaneously wash, concentrate and disperse the nanocomposite particles.

4.2.1. Silane coupling agents and dispersants

The first step in the dispersion procedure is to modify nanoparticle surfaces with a silane coupling agent or other dispersant.[143] This electrostatic protection method of dispersion utilizes the high surface areas characteristic of nanoparticles.[2,150] The dispersant consists of an anchor group which binds to nanoparticle surfaces and a charged terminal group such as $–NH_3^+$ extends into solution in order to overcome attractive van der Waals forces present in nanoparticle systems. The electrostatic dispersion provided by the small organic and inorganic absorbates is also sensitive to solution pH with pH values in the range of pH 6.5 found to be most efficient.[151]

APS has been utilized as the dispersant in AMA nanocomposite syntheses in prior studies.[131,143,144] The AMA nanocomposite particle surfaces were treated with 1 w/o dispersant solution.[131] After APS surface modification, the particle surfaces are positively charged (~ +30 mV) at pH~6.5. Other dispersants can also be used including trimethoxysilylpropyl-diethylenetriamine (DETA), sodium citrate dihydrate and combinations of dispersants.[149]

Electrostatic dispersion is metastable to agglomeration, particularly in relatively high ionic strength solutions such as 0.01M NaCl, thus additional washing and dispersion steps are required.[30] Additionally, in this dispersion regime, agglomerated particles cannot be redispersed.[30] Nevertheless, electrostatic dispersion via surface modification of the AMA nanocomposite particles is useful since it enhances the effectiveness of HPLC washing.

4.2.2. Size-exclusion high performance liquid chromatography

Size-exclusion high performance liquid chromatography (HPLC) generates stable unagglomerated nanocomposite particle suspensions superior to other particle recovery techniques including sedimentation, centrifugation or Soxhlet extraction with displacement washing.[131] The HPLC washing procedure is based on an analytical technique used for the separation of complex liquids. HPLC washing removes surfactant and other precursors as well as any unencapsulated fluorescent or therapeutic agents. The separation of the nanoparticles from the waste-containing carrier solution is achieved due to differences in the interactions of the mobile and stationary phases.[152,153]

The nanocomposite particles are washed and dispersed using a size-exclusion HPLC system* illustrated in Figure 4.4. An unpacked HR 5/5 (5 x 50 mm) HPLC column was purchased from Amersham Biosciences (Piscataway, NJ). The column is packed with 20 μm (bare or APS-treated) spherical silica beads purchased from Stellar Phases Inc. (Langhorne, PA). Dehydrated ethanol (pH adjusted to nanoparticulate system requirements using acetic acid) is pumped through the HPLC to wet the column packing before the nanoparticle suspension is introduced. In the HPLC washing procedure, the nanoparticle suspension is pumped into the HPLC system through a stationary phase at a flow rate of 1 mL/min. The end of the HPLC after the packed column is connected to detectors in order to measure UV absorbance or fluorescence.[131] The detectors are used to monitor when the column is fully saturated with nanoparticles. The particles are eluted and redispersed using an ethanol/ distilled water solution of up to 70 v/o water.

** Waters Delta Preparation 3000 HPLC System, Milford, MA*

FIGURE 4.4 - Schematic of the HPLC system used to wash and disperse nanoparticles.

The HPLC washing and dispersion process is influenced by numerous processing variables including surface modification of the mobile and stationary phases, suspension pH, elutant solution composition, flow rate and column dimensions.[131,152,153] Typically, nanocomposite particle suspensions between 10-20 w/o solids loading are obtained as measured by acoustic methods.[154]

4.2.3. Nano-suspension dispersion characterization

Unagglomerated AMA nanocomposite suspensions were attained based on characterization techniques including quasi-elastic light scattering (QELS)*, transmission electron microscopy (TEM)** and atomic force microscopy (AFM)*** . Additionally, zeta potential measurements were conducted using

** Nano S Zetasizer, Malvern Instruments Ltd., UK*
*** JEOL 2010F high-resolution-TEM, Japanese Electronics and Optics Laboratory, Tokyo, Japan*
**** MultiMode, Digital Instruments, Veeco Instruments*

electrophoretic light scattering*. The AMA nanocomposite suspension pH was measured using a Sentron pH meter**. Density measurements were performed using an acoustic hand-held density meter to determine the solids loading of the washed nanocomposite suspensions***.

The state of dispersion of the AMA nanosuspensions can be characterized using the average agglomeration number (AAN) defined earlier.[2,68,155] The AAN is calculated from the ratio of the median particle volume determined via QELS to the microscopic particle size volume determined through TEM analysis.[2,68,155] An AAN <10 indicates a well-dispersed suspension.[2,68,155]

The state of dispersion of a nanocomposite Rhodamine B/SiO_2 suspension was analyzed using the AAN approach. The sample (SMR 3-69) parameters are R=4, H=100, X=1. Figure 4.5 shows the nanosuspension characterization using QELS which provided a particle size of 32.0 nm. Characterization by TEM gives a particle size of 25.5 nm ± 4.50 nm in good agreement with the QELS particle size. Figure 4.6 shows a typical nanoparticle from the sample.

** ZetaPALS, Brookhaven Instrument Corp., Holtsville, NY*
*** Argus IP 65 ISFET, Sentron Inc.,The Netherlands*
**** Anton Paar, DMA 35N, Graz, Austria*

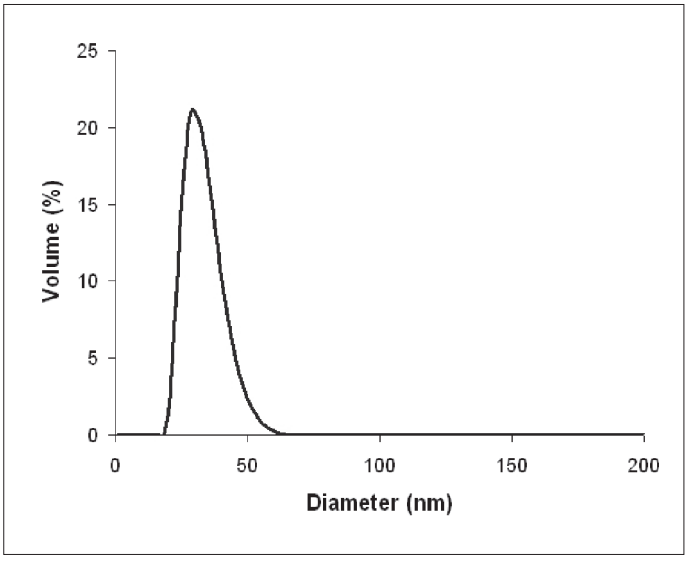

FIGURE 4.5 - Plot of Rhodamine B/SiO_2 nanoparticle size distribution by volume.

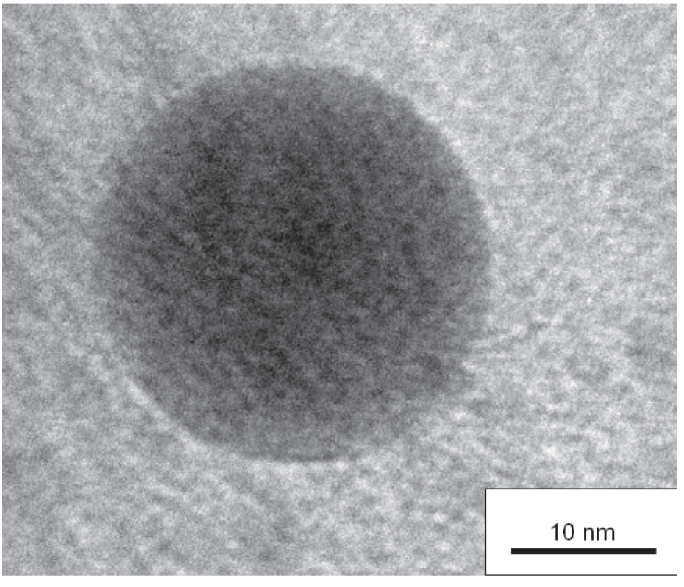

FIGURE 4.6 - TEM image of Rhodamine B/SiO_2 nanoparticle.

The AAN for the Rhodamine B/SiO_2 nanosuspension is 2.0. Thus, the suspension can be classified as well-dispersed. The discrepancy in particle sizes given by QELS and TEM is due at least in part to the QELS measurement of the electrical double layer surrounding each of the nanocomposite particles leading to a larger particle size measurement. Instrumental broadening also occurs in QELS particle size determinations. We are currently developing a standard protocol for the QELS for the nanocomposite colloidal suspensions to minimize hydrodynamic radius effects due to double layer sensitivity.

4.3. Nanomedical applications

Stable, highly dispersed and unagglomerated core shell-matrix nanoparticles can be used for a variety of biomedical applications including bioimaging, drug delivery, gene therapy and combinations of bioimaging during active medical agent delivery. Size, surface chemistry and dispersion contribute to the effectiveness of the AMA nanocomposite particles as biomedical tools.

4.3.1. BioImaging

Nanocomposite particles doped with organic fluorophores have the potential to circumvent various functional limitations encountered by

traditional organic dyes and other new bioimaging tools, such as quantum dots (marketed as Q-dots™).[126,156-158] Fluorescent labeling of biological materials using small organic dyes is extensively utilized in a variety of applications including diagnostics and biological imaging. However, many characteristics of organic fluorophores limit the effectiveness of organic fluorophores for such applications. High concentrations of dye molecules are often required for bioimaging, as the fluorophore will eventually bleach due to photo-physical degradation.[149] Thus, experiments with organic dyes are often limited to short time periods due to the short lifetimes of the organic fluorophores.[159] Furthermore, organic fluorophores rapidly self-quench which limits the dye concentration that can be introduced to the system.[159]

There have been numerous advances in the development of colloidal fluorescent semiconductor nanocrystals, or quantum dots (QDs), such as ZnS shell-CdSe cores, used for bioimaging. Research indicates that QDs can be of benefit as biological labels, when compared to the existing organic dyes.[126,149,157] However, QD emissions are strongly intermittent and agglomeration can limit their effectiveness as a bioimaging tool.[40] Additional problems associated with QDs include surface electronic defects and toxicological effects as surface oxidation can cause degradation of the QD, releasing toxic heavy metals into the body.[160,161]

The nanocomposite particles exhibit strong size-dependent emission spectra due to quantum size effects.[134] Furthermore, the nanoparticles have virtually continuous excitation spectra above the threshold for absorption. As a result, the photoluminescence from the nanocomposite particles can be detected at lower dye concentrations than that for organic dyes by conventional fluorescence methods, with the benefit of biocompatibility.[127,162] The fluorescent nanocomposite particles may be used to examine capillary flow, define neuronal cell connectivity and to study translocations through gap junctions.

The shell matrix can consist of SiO_2, $CaPO_4$, CPS or TiO_2, the last material an inherent, inorganic, bactericidal material. Numerous organic fluorophores have been encapsulated including the sodium salt of fluorescein, Rhodamine 123, Rhodamine B, Indocyanine Green, (Aldrich Chemical Co., Milwaukee, WI). Rhodamine WT (Presto Dye Chem Co., Philadelphia, PA), cascade blue acetyl azide (Molecular Probes, Inc. Eugene, OR), Cy 3 Amidite, and Cy 5 amidite (Amersham Biosciences, Piscataway, NJ).

The fluorescent nanocomposite particle structure includes an organic fluorophore doped inside a silica nanoporous network as shown in Figure 4.7. Direct contact between dye molecules and the environment is avoided, eliminating photodegradation of the fluorophore presumably because of absorption of the most energetic, and therefore, damaging of the excitation

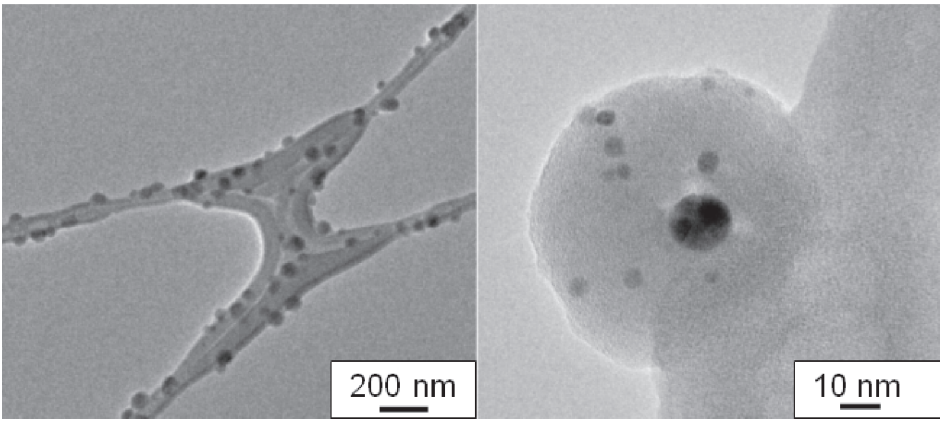

FIGURE 4.7 - TEM images of Rhodamine WT/SiO_2 nanoparticles. (TEM photomicrograph courtesy of J.A. Nelson).

photons. As a result, the nanoparticles exhibit extended fluorescence lifetimes relative to traditional organic fluorophores or the QDs.

The nanoparticles possess high resistance to photodegradation due to the protection of the fluorescent core provided by the encapsulating matrix. Figure 4.8 includes three successive scans conducted on the F-4010 Fluorescence Spectrophotometer (Hitachi, Ltd., Japan) to determine the susceptibility of the fluorescein/SiO_2 nanoparticles to photobleaching. The shift in the emission peak and the inhibition of photobleaching verifies that the organic fluorophore has been encapsulated. The nanoparticles containing 1 M fluorescein encapsulated in SiO_2 exhibit intensities 200% greater than that for free fluorescein in solution without self-quenching. The small peaks at 475 nm indicate the excitation setting for each sample and are due to scattered excitation light.

Schott Nexterion AG (S. Conzone, Dueyea, PA) performed an independent experiment to examine the fluorescent character of the nanocomposite particles. Figure 4.9 shows the results of the experiments. The nanoparticle solutions were printed (10 spots per row per 8 samples) on a SCHOTT epoxy slide using GeneMachines OmniGrid Accent microarrayer. The slide was scanned in the Axon scanner at 100% laser power 30 consecutive times. The multiple scans with high intensity laser verified that not only do the nanocomposite particles resist photodecay, they also exhibit an enhancement in fluorescent emission when excited by a high power laser. The fluorescent character of a variety of core-shell QD nanocomposite particles was also examined, including CdS shell/CdSe core quantum dots. The QD

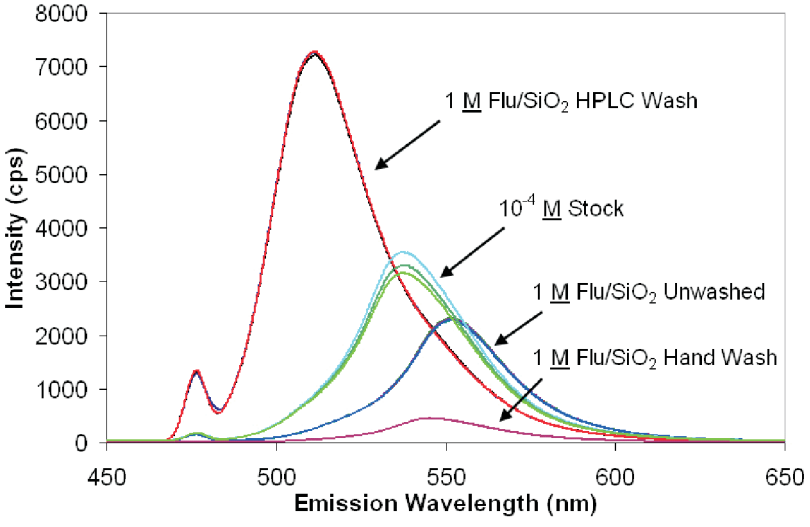

Figure 4.8 - Fluorescent emission scan of fluorescein/SiO_2 nanoparticles.

	Percent Decrease (from Scan 1 to 30)		
	FLUOROPHORE	% difference	
1	Sarah 3-90 RhB/SiO2 Et	-	8.37%
2	Sarah 2-94 RhB/Et SiO2	+	0.51%
3	Sarah 2-90 RhB/Et SiO2	+	4.25%
4	EIA 1-08 RhWT/SiO2	-	5.21%
5	SMR 5-74 F/SP IT	+	14.94%
6	Sarah 4-44 F/SiO2	+	2.85%
7	Sarah 4-33 F/SiO2	+	1.00%
8	Ag/SiO2	-	1.76%
	key	" - " = decrease	
		" + " = increase	

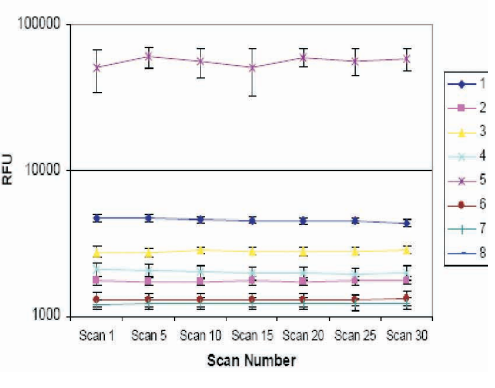

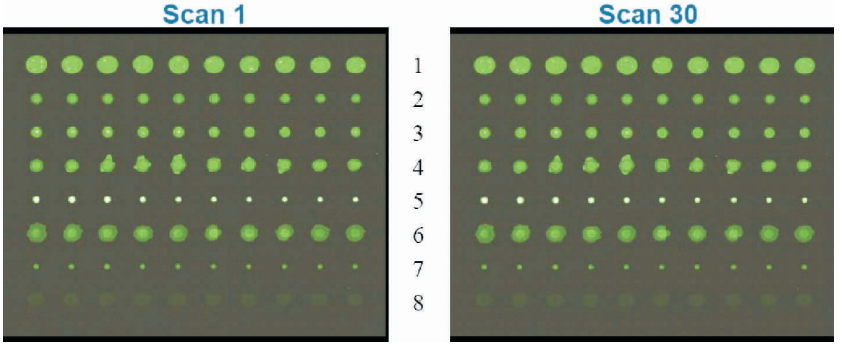

FIGURE 4.9 - Nanocomposite particle photodecay experiment results. (Data courtesy of S. Conzone, Schott Nexterion AG, Dueyea, PA).

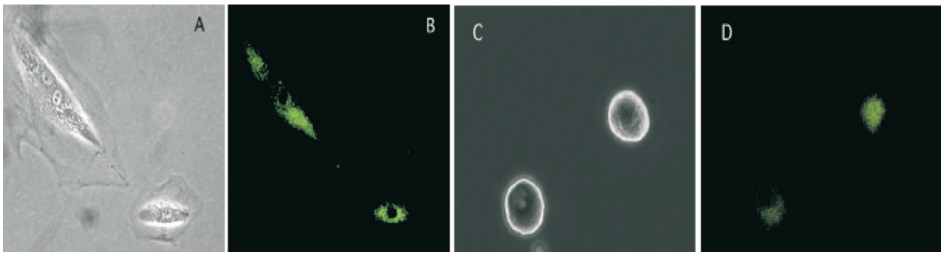

FIGURE 4.10 - Phase contrast (A) and fluorescent image (B) of cultured vascular A7r5 smooth muscle cells that have taken up fluorescein/SiO_2 nanoparticles. Phase image (C) and fluorescent image (D) of acutely isolated rat stellate ganglia neurons five days following intracardial injection of the nanoparticles. (Data courtesy of Victor-Ruiz-Velasco, Hershey Medical Center, Hershey, PA).

arrays (not shown) lost approximately 50% emission intensity due to photodegradation during the 30 scan experiment.

The fluorescent nanoparticles' effectiveness as a bioimaging tool was also examined by Victor Ruiz-Velasco at Hershey Medical Center, Hershey, PA. Figure 4.10 shows cultured vascular A7r5 smooth muscle imaged using fluorescein/SiO_2 nanoparticles. It was observed that fluorescein/SiO_2 nanoparticles (0.002% 1 M) induce fluorescence of 100% of cultured A7r5 vascular smooth muscle cells without inducing apoptosis. Additional experiments performed at Hershey Medical Center showed that acutely isolated cardiac neurons displayed identical electrophysical properties as unlabeled control neurons, which indicates that the fluorescent nanoparticles do not cause significant adverse toxicological effects. In contrast, studies indicated that quantum dots were lethal in all neurons tested within 10-15 minutes of use under *in vitro* conditions. Additionally, the organic fluorophore/SiO_2 nanoparticles were also non-toxic in cell culture models. At a nanoparticle concentration 100-fold higher than employed in cell culture experiments, no acute or chronic toxicity was induced in Swiss Webster mice.

4.4. Conclusions

The research presented provides a method for the synthesis of stable, unagglomerated nanocomposite particles. The nanoparticles consist of active medical agent(s) encapsulated in a variety of shell matrix materials. Dispersion of the nanocomposite particles is achieved using electrostatic dispersion techniques in conjunction with size-exclusion HPLC to simultaneously launder and concentrate while maintaining dispersed nanocomposite particles. The

AMA nanocomposite particles have been evaluated using average agglomeration (AAN) theory in conjunction with other characterization techniques and through experiments performed at Hershey Medical Center. The nanocomposite particles can be used in a variety of nanomedical applications including bioimaging, drug delivery and possibly gene therapy.

REFERENCES

1. W. Ostwald and H.W. Morse, "Elementary Modern Chemistry", *The Atbenaum Press*, 1-291 (1909).
2. R. Zsigmondy, E.B. Spear, "The Chemistry of Colloids", *John Wiley & Sons, Inc.,* 1-288 (1917).
3. T. Svedberg, "Colloid Chemistry", *The Chemical Catalog Company, Inc.,* 1-302 (1928).
4. M. Faraday, "Experimental Researches in Chemistry and Physics," *Taylor and Francis*, 1-496 (1991).
5. H.R. Kruyt, "Colloid Science", *Elsevier Publishing Company*, **1**, 1-389 (1952).
6. D.C. Grahame, "The Electrical Double Layer and the Theory of Electrocapillarity", 441-501 (1945).
7. E.J.W. Verwey and J.Th.G. Overbeek, "Theory of the Stability of Lyophobic Colloids", *Elsevier Publishing Company, Inc.*, 1-205 (1948).
8. A.E. Alexander and P. Johnson, "Colloid Science", *Oxford at the Clarendon Press*, 1-852 (1949).
9. I.E. Dzyaloshinskii, E.M. Lifshitz and L.P. Pitaevskii, "The General Theory of van der Waals Forces", Institute of Physical Problems of the U.S.S.R, Academy of Sciences, Moscow, 165-209 (1961).
10. R. Hogg, T.W. Healy, and D.W. Fuerstenau, "Mutual Coagulation of Colloidal Dispersions", Department of Mineral Technology, University of California, Berkeley, CA, 1638-1651 (1965).
11. E.A. Guggenheim, "Thermodynamics – An Advanced Treatment for Chemists and Physicists", *Elsevier Science Publishers*, 1-390 (1967).
12. H. Krupp, "Particle Adhesion – Theory and Experiment", *Advanced Colloid Interface Science*, **1,** 79-110 (1967).
13. J.N. Israelachvili and B.W. Ninham, "Intermolecular Forces – The Long and Short of it", *Journal of Colloid and Interface Science*, **58** [1] 14-25 (1977).
14. G.Y. Onoda, Jr., and L.L. Hench, "Ceramic Processing Before Firing", *John Wiley & Sons, Inc.*, 1-490 (1978).
15. R.K. Iler, "The Chemistry of Silica – Solubility, Polymerization, Colloid and Surface Properties, and Biochemistry", *John Wiley & Sons, Inc*., 1-866 (1979).

16. D.B. Hough and L.R. White, *Advances in Colloid and Interface Science* **14,** 3-41 (1980).
17. R.J. Hunter, "Zeta Potential in Colloid Science - Principles and Applications", *Academic Press*, 1-386 (1981).
18. R.J. Hunter, "Foundations of Colloid Science", *Clarendon Press*, **1**, 1-673 (1986).
19. R. Vold and M.J. Vold, "Colloid and Interface Chemistry," *Addison-Wesley Publishing Company, Inc.*, 1-694 (1983).
20. D.H. Napper, "Polymeric Stabilization of Colloidal Dispersions", *Academic Press*, 1-428 (1983).
21. D.H. Solomon and D.G. Hawthorne, "Chemistry of Pigments and Fillers", *John Wiley & Sons*, 1-309 (1983).
22. S. Ross and I.D. Morrison, "Colloidal Systems and Interfaces", *John Wiley & Sons, Inc.,* 1-422 (1988).
23. W.B. Russel, D.A. Saville, and W. R. Schowalter, "Colloidal Dispersions", *Press Syndicate of the University of Cambridge*, 1-525 (1989).
24. R.J. Hunter, "Foundations of Colloid Science", *Oxford Science Publications*, **2**, 1-1089 (1989).
25. A.W. Adamson, "Physical Chemistry of Surfaces", *John Wiley & Sons, Inc.*, Fifth Edition, 1-777 (1990).
26. J. Israelachvili, "Intermolecular and Surface Forces", *Academic Press*, 1-450 (1992).
27. J.H. Adair, J.A. Casey, and S. Venigalla, "Handbook on Characterization Techniques for the Solid-Solution Interface", *The American Ceramic Society*, 1-300 (1993).
28. P.C. Hiemenz and R. Rajagopalan, "Principles of Colloid and Surface Chemistry," Third Edition, *Marcel Dekker, Inc*. 1-650 (1997).
29. B.M. Moudgil and P. Somasundaran, "Dispersion and Aggregation - Fundamentals and Applications," *Proceedings of the Engineering Foundation Conference,*1-583 (1992).
30. J.H. Adair, E. Suvaci, and J. Sindel, "Surface and Colloid Chemistry of Advanced Ceramics," *Encyclopedia of Materials: Science and Technology*, Elsevier Publishing, The Netherlands, 8996-9006 (2001).
31. John Green, DuPont Nemours, Private communications. Used with permission.
32. G.L. Messing, The Pennsylvania State University, University Park, PA, 16802, private communication.
33. G.L. Messing, K.S. Mazdiyasni, J.W. McCauley, and R.A. Haber, "Advances in Ceramics – Ceramic Powder Science", The American Ceramic Society, 21, 1-825 (1987).
34. G.L. Messing, E.R. Fuller, Jr., and H. Hausner, "Ceramic Powder Science II, A", *The American Ceramic Society, Inc.,* **1**, 1-591 (1988).

35. G.L. Messing, E.R. Fuller, Jr., and H. Hausner, "Ceramic Powder Science II, A", *The American Ceramic Society, Inc.,* **1**, 1-1207 (1988).
36. J.S. Reed, "Introduction to the Principles of Ceramic Processing", *John Wiley & Sons, Inc.,* 1-486 (1988).
37. G.L. Messing, S. Hirano, and H. Hausner, "Ceramic Powder Science III", *The American Ceramic Society,* **12**, 1-995 (1990).
38. R.J. Pugh, and L. Bergström, "Surface and Colloid Chemistry in Advanced Ceramics Processing," *Marcel Dekker*, Inc., **51**, 1-363 (1994).
39. J.H. Adair, J.A. Casey, C.A. Randall, and S. Venigalla, "Science, Technology, and Applications of Colloidal Suspensions", *American Ceramic Society*, **54** 1-278 (1995).
40. T.A. Ring, "Fundamentals of Ceramic Powder Processing and Synthesis", *Academic Press*, 1-961 (1996).
41. A. Jillavenkatesa and G.Y. Onoda, "Advances in Process Measurements for the Ceramic Industry", *The American Ceramic Society,* 1-397 (1999).
42. R.H. French, R.M. Cannon, L.K. DeNoyer, and Y.M. Chiang, "Full Spectral Calculations of Non-Retarded Hamaker Constants for Ceramic Systems from Interband Transition Strengths," Solid State Ionics, vol. **75**, 13-33 (1995).
43. L. Bergstrom, "Hamaker Constants of Inorganic Materials," Adv. Colloid Int. Sci., 70, 125-169 (1997).
44. M.M. Mandanas, *Ph.D. Thesis: Colloidal Approach to Dispersion and Enhanced Deaggregation of Aqueous Ferrite Suspensions*. University Park: The Pennsylvania State University, (2001).
45. S.M. Gatica, M.W. Cole, and D. Velegol, "Designing van der Waals Forces between Nanocolloids," Nano Letters, **5** [1], 169-173 (2005).
46. J.H. Adair, T. Li, T. Kido, K. Havey, J. Moon, J. Mecholsky, A. Morrone, D. R. Talham, M.H. Ludwig, and L. Wang, "Recent Developments in the Preparation and Properties of Nanometer-Size Spherical and Platelet-Shaped Particles and Composite Particles", *Elsevier Sciences, Inc.,* **R23** 139-242 (1998).
47. F.F. Lange, "Powder Processing Science and Technology for Increased Reliability," *Journal of American Ceramic Society*, **72**, 3-15 (1989).
48. W.M. Sigmund, N.S. Bell, and L. Bergstrom, "Novel Powder-Processing Methods for Advanced Ceramics," *Journal of American Ceramic Society*, **83**, 1557-1574 (2000).
49. J.M. McHale, A. Navrotsky, and A.J. Perrotta, "Effects of Increased Surface Area and Chemisorbed H_2O on the Relative Stability of Nanocrystalline γ-Al2O3 and α-Al2O3," *Journal of Physical Chemistry-B*, **101**, 603-613 (1997).
50. K.C. Hass, W.F. Schneider, A. Curioni, and W. Andreoni, "The Chemistry of Water on Alumina Surfaces: Reaction Dynamics from First Principals,"

Science, **282**, 265-268 (1998).
51. A. Maskara and D.M. Smith, "Agglomeration during the Drying of Fine Silica Powders, Part II: The Role of Particle Solubility," *Journal of American Ceramic Society*, **80**, 1715-1722 (1997).
52. S. Kwon and G.L. Messing, "The Effect of Particle Solubility on the Strength of Nanocrystalline Agglomerates: Boehmite," *Nanostructured Materials*, **8**, 399-418 (1997).
53. M. Kitayama and J.A. Pask, "Formation and Control of Agglomerates in Alumina Powder," *Journal of American Ceramic Society*, **79**, 2003-2011 (1996).
54. C.J. Brinker and G.W. Scherer, *Sol-Gel Science: The Physics and Chemistry of Sol-Gel Processing*. San Diego: Academic Press, Inc., (1990).
55. R. Kumar, J.O. Sofo, K. Sutovich, T.G. Roberie, and J.H. Adair, "Effect of Surface Hydration on Aggregation of Alumina Clusters," *Under Preparation*, (2005).
56. W. Peukert, H.C. Schwarzer, and F. Stenger, "Control of aggregation in production and handling of nanoparticles," *Chemical Engineering and Processing*, **44**, 245-252 (2005).
57. J.A. Lewis, "Colloid Processing of Ceramics," *Journal of American Ceramic Society*, **83,** 2341-2359 (2000).
58. S. Kwon, C.S. Nordahl, and G.L. Messing, "Consolidation of Nano-Crystalline Alumina," *Materials and Manufacturing Processes*, **11**, 969-985 (1996).
59. L.G. Austin and R.R. Klimpel, "The Theory of Grinding," *Industrial and Engineering Chemistry*, **56**, 18-29 (1964).
60. B. Beke, *The Process of Fine Grinding*, vol. 1. Boston: Martinus Nijhoff/ Dr W. Junk Publishers, (1981).
61. A. Kwade, "Mill selection and Process Optimization Using a Physical Grinding Model," *International Journal of Mineral Processing*, **74S**, S93-S101 (2004).
62. R. Kumar, N. Antolino, E. Wichard, K. Sutovich, T.G. Roberie, and J.H. Adair, "Optimized De-aggregation and Dispersion of High Concentration Slurry of Nanophase Alumina by Chemically Aided Attrition Milling," *Under Preparation*, (2005).
63. W.B. Hillig and R.J. Charles, "Surfaces, Stress-Dependent Surface Reactions, and Strength," in *High-Strength Materials*, V.F. Zackay, Ed. New York: Wiley, (1964).
64. T.A. Michalske and B.C. Bunker, "Stress Corrosion of Ionic and Mixed Ionic/Covalent Solids," *Journal of American Ceramic Society*, **69**, 721-724 (1986).
65. T.A. Michalske and B.C. Bunker, "Steric effects in Stress Corrosion

Fracture of Glass," *Journal of American Ceramic Society*, **70**, 780-784 (1987).
66. J.H. Adair, T.R. Shrout, G.L. Messing, T.H. Pecora, and M.M. Mandanas, "Dynamic Control and Enhanced Chemical Milling of Ceramics to Submicron Particle Sizes," in *US Patent # 6,415,996*. United States of America, (2002).
67. C.F. Baes and R.E. Mesmer, "The Hydrolysis of Cations." New York: Wiley, 112-123 (1976).
68. H.G. Krarup, M.M. Mandanas, and J.H. Adair, "Physical Characterization of Fine Powders," *Fine Powder Processing - International Conference Proceedings*, 63-70 (1999).
69. A. Szegvari and M. Yang, "Attritor Grinding and Dispersing Equipment," Union Process, Inc., Akron, OH (1999).
70. M. Pechini, U.S. Patent No. 3,330,697, July 1967.
71. Ch. Laberty-Robert, F. Ansart, C. Deloget, M. Gaudon, and A. Rousset, "Powder Synthesis of Nanocrystalline ZrO_2-8%Y_2O_3 Via a Polymerization Route," *Mater. Res. Bull.*, **36**, 2083-2101 (2001).
72. J.A. Wang, M.A. Valenzuela, J. Salmones, A. Vazquez, A. Garcia-Ruiz, and X. Bokhimi, "Comparative Study of Nanocrystalline Zirconia Prepared by Precipitation and Sol-gel Methods," *Catalysis Today*, **68**, 21-30 (2001).
73. A.P. Oliveira and M.L. Torem, "The Influence of Precipitation Variables on Zirconia Powder Synthesis," *Powder Technology*, **119**, 181-193 (2001).
74. M. Li and G.L. Messing, "Preparation of Spherical Zirconia Particles by Controlled Coagulation in Zirconia Sols"; pp. 129-136 in Ceramic Transactions, Vol. 12, *Ceramic Powder Science III*. Edited by G.L. Messing, E.R. Fuller, Jr and H. Hausner. The American Ceramic Society, Westerville, OH, (1990).
75. G. Rinn and H. Schmidt, "Preparation of Monodispersed Zirconia Powders from Solution"; pp. 23-30 in Ceramic Transactions, Vol. 1, *Ceramic Powder Science III: A*. Edited by G.L. Messing, E.R. Fuller, Jr and H. Hausner. The American Ceramic Society, Westerville, OH, (1987).
76. M.H. Lee, C.Y. Tai and C.H. Lu, "Synthesis of Spherical Zirconia by Precipitation Between Two Water/Oil Emulsions, " *J. Eur. Ceram. Soc.*, **19**, 2593-2603 (1999).
77. W. Li and L. Gao, "Nano ZrO_2 (Y_2O_3) Particles Processing by Heating of Ethanol-Aqueous Salt Solutions," *Ceramics International*, **27**, 543-546 (2001).
78. B. Xia, L. Duan and Y. Xie, "ZrO2 Nanopowders Prepared by Low-Temperature Vapor-Phase Hydrolysis," *J. Am. Ceram. Soc.*, **83** [5], 1077-1080 (2000).
79. T. Tsukada, S. Venigalla, A.A. Morrone and J.H. Adair, "Low-Temperatu-

re Hydrothermal Synthesis of Yttrium-Doped Zirconia Powders," *J. Am. Ceram. Soc.*, **82** [5], 1169-1174 (1999).
80. E.P. Stambaugh, J.H. Adair, I. Sekercioglu and R.R. Wills, "Hydrothermal Method for Producing Stabilized Zirconia," U.S. Patent No. 4,619,817, October 28, 1986.
81. R.P. Denkewicz, K.S. TenHuisen and J.H. Adair, "Hydrothermal Crystallization Kinetics of *m*-ZrO_2 and *t*-ZrO_2," *J. Mater. Res.*, **5**, 2698-2705 (1990).
82. H. Vesteghem, I. Charissou and H. Reveron, "Hydrothermal Synthesis of Colloidal Zirconia," *Key Engineering Materials*, **132-136**, 129-132 (1997).
83. M. Yoshimura and S. Somiya, "Fine Zirconia Powders by Hydrothermal Processing," Report of the Research Laboratory of Engineering Materials, Tokyo Institute of Technology, *Number 9*, 1984.
84. G. Dell'Agli and G. Mascolo, "Agglomeration of 3 mol% Y-TZP Powders Synthesized by Hydrothermal Treatment," *J. Eur. Ceram. Soc.*, **21** [1], 29-35 (2001).
85. O. Vasylkiv and Y. Sakka, "Hydroxide Synthesis, Colloidal Processing and Sintering of Nanosized 3Y-TZP Powder," *Scripta mater.*, **44**, 2219-2223 (2001).
86. R.R. Piticescu, C. Monty, D. Taloi, A. Motoc and S. Axinte, "Hydrothermal Synthesis of Zirconia Nanomaterials," *J. Eur. Ceram. Soc.*, **21**, 2057-2060 (2001).
87. Y.B. Khollam, A.S. Deshpande, A.J. Patil, H.S. Potdar, S.B. Deshpande and S.K. Date, "Synthesis of Yttria Stabilized Cubic Zirconia (YSZ) Powders by Microwave-Hydrothermal Route," *Materials Chemistry and Physics*, **71**, 235-241 (2001).
88. V.K. LeMer and R.H. Dinegar, "Theory, Production and Mechanism of Monodispersed Hydrosols," *J. Am. Chem. Soc.*, **72** [11], 4847-4854 (1950).
89. H.H. Willard, "Separation by Precipitation from Homogeneous Solution," *Anal. Chem.*, **22**, 1372-1374 (1950).
90. B.I. Intorre and A.E. Martell, "Zirconium Complexes in Aqueous Solution. I. Reaction With Multidentate Ligands," *J. Am. Chem. Soc.*, **82** [1], 358-364 (1960).
91. B.I. Intorre and A.E. Martell, "Zirconium Complexes in Aqueous Solution. II. Mixed Chelates," *J. Am. Chem. Soc.*, **83** [9], 3618-3623 (1961).
92. B.I. Intorre and A.E. Martell, "Zirconium Complexes in Aqueous Solution. III. Estimation of Formation Constants," *Inorganic Chemistry*, **3** [1], 81-87 (1964).
93. J.H. Adair, J.A. Kerchner, N.S. Bell and M.L. Carasso, "Application of Chemical Principles in the Solution Synthesis and Processing of Ceramic

and Metal Particles"; chap. 9 in Synthesis and Characterization of Advanced Materials (symposium, Orlando, FL, August 1996). Edited by M.A. Serio, D.M. Gruen and R. Malhortra. American Chemical Society, Washington, DC.

94. H.C. Chang, T.W. Healy and E. Matijevic, "Interactions of Metal Hydrous Oxides with Chelating Agents. III. Adsorption on Spherical Colloidal Hematite Particles," *Journal of Colloid and Interface Science*, **92** [2], 469-478 (1983).
95. R.P. Denkewicz, K.S. TenHuisen and J.H. Adair, "Hydrothermal Crystallization Kinetics of *m*-ZrO_2 and *t*-ZrO_2," *J. Mater. Res.*, **5**, 2698-2705 (1990).
96. R.A. Kimel and J.H. Adair, "Recovery of Well-Dispersed Less Than 10 nm Y-TZP Utilizing a Nanoscale Analog to a Protective Colloid Approach," to be submitted.
97. R.A. Kimel and J.H. Adair, "Aqueous Degradation and Chemical Passivation of Yttria Tetragonally Stabilized Zirconia at 25°C," *Jour. Amer. Ceram. Soc.*, **85** [6], 1403-1408 (2002).
98. M.J. Mayo, "Nanocrystalline Ceramics for Structural Applications: Processing and Properties,"*Nanostructured Materials: Science and Technology*, Chap. 18, edited by G-M. Chow. Dordrecht, The Netherlands: Klewer, (1998).
99. A.O. Boschi and E. Gilbart, "Wet Forming Processes as a Potential Solution to Agglomeration Problems," *Advanced Ceramic Processing and Technology 1*, edited by J.G.P. Binner. Park Ridge, NJ: Noyesd Publications, 73-93 (1990).
100. H. Nienburg and F. Harbach, "Pressure Filtration of Fine Ceramic Suspensions," *Ceramic Powder Science IV*, edited by S. Hirano, G.L. Messing, and H. Hausner. Westerville, OH: American Ceramic Society, 321-327 (1991).
101. B.E. Novich and D.H. Pyatt, "Consolidation Behavior of High-Performance Ceramic Suspensions," *Jour. Amer. Ceram. Soc.*, **73** [2], 207-212 (1990).
102. G. Skandan, H. Hahn, B.H. Kear, M. Roddy and W.R. Cannon, "The Effect of Applied Stress on the Densification of Nanostructured Zirconia During Sinter-Forging," *Materials Letters*, **20**, 305-309 (1994).
103. C.D. Sagel-Ransijn, A.J. Winnubst, B. Kerwijk, A.J. Burggraaf and H. Verweij, "Production of Defect-Poor Nanostructured Ceramics of Yttria-Zirconia," *Jour. Eur. Ceram. Soc.*, **17**, 831-841 (1997).
104. B.V. Velamakanni and F.F. Lange, "Effect of Interparticle Potentials and Sedimentation on Particle Packing Density of Bimodal Particle Distributions During Pressure Filtration," *Jour. Amer. Ceram. Soc.*, **74** [1], 166-172 (1991).

105. F.F. Lange and K.T. Miller, "Pressure Filtration: Consolidation Kinetics and Mechanics," *Amer. Ceram. Soc. Bull.*, **66** [10], 1498-1504 (1987).
106. I.A. Aksay, "Molecular and Colloidal Engineering of Ceramics," *Ceramics International*, **17**, 267-274 (1991).
107. A. Lang, "The Role of Dissolution in Pressure Filtration of Yttria Stabilized Nanocrystalline Zirconia"; B.S. Thesis, The Pennsylvania State University, University Park, December 1998.
108. R.A. Kimel "Solution Chemistry Issues During the Aqueous Synthesis and Processing of Nanosized Yttria Tetragonally Stabilized Zirconia (YTZP)"; Ph.D. Thesis. The Pennsylvania State University, University Park, PA. August 2002; Chapter 6.
109. D.V. Miller and J.S. Reed, "Packing Density of Alumina Blends for Substrates Evaluated from Pressure Filtered-Pressed Compacts,"; pp. 733-740 in Ceramic Transactions, Vol. 1, *Ceramic Powder Science II*. Edited by G.L. Messing, E.R. Fuller, Jr and H. Hausner. The American Ceramic Society, Westerville, OH, (1988).
110. C.H. Shilling, W.H. Shih, and I.A. Askay, "Advances in the Drained Shaping of Ceramics,"; pp. 307-320 in Ceramic Transactions, Vol. 22, *Ceramic Powder Science IV*. Edited by S. Hirano, G.L. Messing, and H. Hausner. The American Ceramic Society, Westerville, OH, (1991).
111. J.H.D. Hampton, S.B. Savage, and R.A.L. Drew, "Experimental Analysis of Fine-Particle Migration during Ceramic Filtration Processes," *J. Am. Ceram. Soc.*, **75** [10] 2726-2732 (1992).
112. J.H.D. Hampton, S.B. Savage, and R.A.L. Drew, "Computer Modelling of Filter Pressing and Clogging in a Random Tube Network," *Chem. Eng. Sci.*, **48** [9] 1601-1611 (1993).
113. B.J. Kellett and C.Y. Lin, "Mechanics of Constant-Rate Filter Pressing of Highly Flocculated Slurries," *J. Am. Ceram. Soc.*, **80** [2] 381-393 (1997).
114. C.Y. Lin and B.J. Kellett, "General Observations of Constant Flow Rate Filter Pressing," *J. Am. Ceram. Soc.*, **81** [8] 2093-2108 (1998).
115. I.W. Chen and X.H. Wang, "Sintering Dense Nanocrystalline Ceramics without Final-Stage Grain Growth," *Nature*, **404** [3] 168-171 (2000).
116. P.L. Chen and I.W. Chen, "Sintering of Fine Oxide Powders: I, Microstructural Evolution," *J. Am. Ceram. Soc.*, **79** [12] 3129-3141 (1996).
117. P.L. Chen and I.W. Chen, "Sintering of Fine Oxide Powders: II, Sintering Mechanisms," *J. Am. Ceram. Soc.*, **80** [3] 637-645 (1997).
118. R.A. Kimel and J.H. Adair, in press, 2004.
119. R.A. Kimel, D.J. Green, and J.H. Adair, in press, 2004.
120. C.J. Szepesi and J.H. Adair, unpublished, 2004.
121. ACD ChemSketchTM ver. 5.1, *http://www.acdlabs.com*, 2002.
122. D.A. LaVan, D.M. Lynn, and R. Langer, "Moving Smaller in Drug Discovery and Delivery," *Nature Reviews Drug Discovery*, **1** 77-84

(2002).
123. M.P. Desai, V. Labhasetwar, G. Amidon *et al*, "Gastrointestinal Uptake of Biodegradable Microparticles: Effect of Particle Size," *Pharmaceutical Research*, **13** [12] 1996.
124. J. Kreuter, "Nanoparticulate Systems for Brain Delivery of Drugs," *Advanced Drug Delivery Reviews*, **47** 65-81 (2001).
125. S. Penn, L. He and M.J. Natan, "Nanoparticles for Bioanalysis," *Current Opinion in Chemical Biology*, **7** 609-615 (2003).
126. M. Ozkan, "Quantum Dots and Other Nanoparticles: What Can They Offer to Drug Discovery?" *Drug Discovery Today*, **9** [24] (2004).
127. S.K. Sahoo and V. Labhasetwar, "Nanotech Approaches to Drug Delivery and Imaging," *Drug Discovery Today*, **8** [24] (2003).
128. I. Roy, T.Y. Ohulchanskyy, H.E. Pudavar, "Ceramic-Based Nanoparticles Entrapping Water-Insoluble Photosensitizing Anticancer Drugs: A Novel Drug-Carrier System for Photodynamic Therapy," *Journal of the American Chemical Society*, **125** 7860-7865 (2003).
129. S.M. Moghimi, A.C. Hunter and J.C. Murray, "Long-Circulating and Target-Specific Nanoparticles: Theory to Practice," *Pharmacological Reviews*, **53** [2] 283-318 (2001).
130. S.S. Davis, "Biomedical Applications of Nanotechnology – Implications for Drug Targeting and Gene Therapy," *Trends in Biotechnology*, **15** 217-224 (1997).
131. J. Wang, "Synthesis of Particulates for Functional Applications: Examples of Nanocomposites and Hematite," Ph.D. Thesis, The Pennsylvania State University (2004).
132. R.H. Muller and C.M. Keck, "Challenges and Solutions for the Delivery of Biotech Drugs – A Review of Drug Nanocrystal Technology and Lipid Nanoparticles," *Journal of Biotechnology*, **13** 151-170 (2004).
133. M. Malmsten, Part IV: Applications of Microemulsions "Microemulsions in Pharmaceuticals" pp. 755-772 in *Handbook of Microemulsion Science and Technology*. Edited by P. Kumar and K.L. Mittal, Marcel Dekker, Inc., New York, NY (1999).
134. J.H. Adair, T. Li, T. Kido *et al*, "Recent Developments in the Preparation and Properties of Nanosize Spherical and Platelet-Shaped Particles and Composite Particles," *Materials Science and Engineering Reviews*, **23** [4-5] 139-242 (1998).
135. T. Li, J. Moon, A.A. Morrone *et al*, "Preparation of Ag/SiO2 Nanosize Composites by a Reverse Micelle and Sol-Gel Technique," *Langmuir*, **15** [13] 4328-4334 (1999).
136. F.J. Arriagada and K. Osseo-Asare, "Controlled Hydrolysis of Tetraethoxysilane in a Nonionic Water-in-Oil Microemulsion: A Statistical Model of Silica Nucleation," *Colloids and Surfaces A: Physiochemical and*

Engineering Aspects, **154** 311-326 (1999).
137. W. Tan, S. Santra, P. Zhang *et al*, "*Coated Nanoparticles*" U.S. Patent, No. 6548264 (2003).
138. W. Lian, S. Litherland, H. Badrane, "Ultrasensitive Detection of Biomolecules with Fluorescent Dye-Doped Nanoparticles," *Analytical Biochemistry*, **334** 135-144 (2004).
139. W. Yang, C.G. Zhang, H.Y. Qu *et al*, "Novel Fluorescent Silica Nanoparticle Probe for Ultrasensitive Immunoassays," *Analytica Chimica Acta*, **503** 163-169 (2004).
140. M. Qhobosheane, S. Santra, P. Zhang et al., "Biochemically Functionalized Silica Nanoparticles," *The Analyst*, **126** 1274-1278 (2001).
141. S. Santra, P. Zhang, K. Wang *et al*, "Conjugation of Biomolecules with Luminophore-Doped Silica Nanoparticles for Photostable Biomarkers," *Analytical Chemistry*, **73** 4988-4933 (2001).
142. M. Lal, L. Levy, K.S. Kim *et al*, "Silica Nonobubbles Containing an Organic Dye in a Multilayered Organic/Inorganic Heterostructure with Enhanced Luminescence," *Chemistry of Materials*, **12** 2632-2639 (2000).
143. S.R. Hall, S.A. Davis and S. Mann, "Cocondensation of Organosilica Hybrid Shells on Nanoparticle Templates: A Direct Synthetic Route to Functionalized Core-Shell Colloids," *Langmuir*, **16** 1454-1456 (2000).
144. T. Ung, L.M. Liz-Marazán and P. Mulvaney, "Controlled Method for Silica Coating of Silver Colloids. Influence of Coating on the Rate of Chemical Reactions," *Langmuir*, **14** 3740-3748 (1998).
145. H. Kusuhara and Y. Sugiyama, "Efflux Transport Systems for Drugs at the Blood-Brain Barrier and Blood-Cerebrospinal Fluid Barrier (Part 1)," *Drug Discovery Today*, **6** [3] 150-156 (2001).
146. L. Brannon-Peppas and J.O. Blanchette, "Nanoparticle and Targeted Systems for Cancer Therapy," *Advanced Drug Delivery Reviews*, **56** 1649-1659 (2004).
147. F.J. Arriagada and K. Osseo-Asare, "Synthesis of Nanosize Silica in a Nonionic Water-in-Oil Microemulsion: Effects of the Water/Surfactant Molar Ratio and Ammonia Concentration," *Journal of Colloid and Interface Science*, **211** 210-220 (1999).
148. K. Osseo-Asare and F.J. Arriagada, "Growth Kinetics of Nanosize Silica in a Nonionic Water-in-Oil Microemulsion: A Reverse Micellar Pseudophase Reaction Model," *Journal of Colloid and Interface Science*, **218** 68-76 (1999).
149. S. Santra, K. Wang, W. Tan *et al*, "Development of Novel Dye-Doped Silica Nanoparticles for Biomarker Application," *Journal of Biomedical Optics*, **6** [2] 160-166 (2001).
150. R.A. Kimel, "Aqueous Synthesis and Processing of Nanosized Yttria Tetragonally Stabilized Zirconia," Ph.D. Thesis, The Pennsylvania State

University (2002).
151. V.A. Hackley and C.F. Ferraris, pp. 5-11 in *The Use of Nomenclature in Dispersion Science and Technology*. Special Publication 960-3, National Institute of Standards and Technology, U.S. Department of Commerce and Technology Administration, U.S. Government Printing Office, Washington, DC (2001).
152. J.M. Hawkins, T.A. Lewis, S.D. Loren *et al*, "Organic Chemistry of C60 (Buckminsterfullerene): Chromatography and Osmylation," *The Journal of Organic Chemistry*, **55** [26] 6250-6252 (1990).
153. D.M. Cox, S. Behal, M. Disko *et al*, "Characterization of C60 and C70 Clusters," *Journal of the American Chemical Society*, **113** [8] 2940-2944 (1991).
154. J.A. Bamberger and M.S. Greenwood, "Measuring Fluid and Slurry Density and Solids Concentration Non-Invasively," *Ultrasonics*, **42** 563-567 (2004).
155. J.H. Adair, A.J. Roese, and L.G. McCoy, "Particle Size Analysis of Ceramic Powders," pp. 142-156 *Advances in Ceramics, Volume 11, Processing for Improved Productivity*, The American Ceramic Society, Columbus, OH (1984).
156. P. Mitchell, "Turning the Spotlight on Cellular Imaging," *Nature Biotechnology*, **19** 1013-1017 (2001).
157. X. Michalet, F. Pinaud, T.D. Lacoste *et al*, "Properties of Fluorescent Semiconductor Nanocrystals and Their Application to Biological Labeling" *Single Molecules Review Article,* **2** [4] 261-276 (2001).
158. W.C.W. Chan and S. Nie, "Quantum Dot Bioconjugates for Ultrasensitive Nonisotopic Detection," *Science*, **281** 2016-2018 (1998).
159. A. Hoshino, K. Hanaki, K. Suzuki *et al*, "Applications of T-lymphoma Labeled with Fluorescent Quantum Dots to Cell Tracing Markers in Mouse Body," *Biochemical and Biophysical Research Communications*, **314** 46-53 (2004).
160. A.M. Derfus, W.C.W. Chan and S.N. Bhatia, "Probing the Cytotoxicity of Semiconductor Quantum Dots," *Nano Letters*, **4** [1] 11-18 (2004).
161. A. Hoshino, K. Fujioka, T. Oku *et al*, "Physiochemical Properties and Cellular Toxicity of Nanocrystal Quantum Dots Depend on Their Surface Modification," *Nano Letters*, **4** [11] 2163-2169 (2004).
162. T. K. Jain, I. Roy, T.K. De *et al*, "Nanometer Silica Particles Encapsulating Active Compounds: A Novel Ceramic Drug Carrier," *Journal of the American Chemical Society*, **120** 11092-11095 (1998).

Discussion

M. Yoshimura: It is true that smaller zirconia crystals would take the tetragonal structure rather than the monoclinic one? However, it does not mean that a thermodynamic critical size exists, because some kinetic factors might control the formation of those tetragonal particles. Do you think that the formation of tetragonal particles might be controlled by thermodynamical factors (i.e. critical size)?

J. Adair: As we discussed in prior papers, during hydrothermal synthesis of ZrO_2, solution pH controls the formation of m-ZrO_2 (low pH), t-ZrO_2 that will slowly transfer to m-ZrO_2 (intermediate pH, say pH 5 to pH 9) and persistent t-ZrO_2 (above about pH 9). So long as ZrO_2 is in a saturated aqueous environment, these pH stabilization regimes seem to hold. Garvie was among the first to propose surface energy stabilization of t-ZrO_2. At high pH, the higher surface energy of the m-ZrO_2 leads to metastable formation of the t-ZrO_2 in the Garvie hypothesis. This we have experimentally confirmed (Demkewicz *et al*, JMR, 1990).
In the solid state, the grain size stabilizes the t-ZrO_2 in sintered specimen. In conventional grain size t-ZrO_2 capable of transformation toughening at 25°C, 3 mole percent Y_2O_3 and grain sizes around 300-600 nm are required. At nanoscale grain sizes, considerably less Y_2O_3 or other stabilizing agents, even no additions, can produce t-ZrO_2. However, the loci of transformation temperature and grain size will need to be experimentally determined. It is expected that the appropriate combinations of grain size and temperature will exist for the nanoscale t-ZrO_2 (without dopant) to demonstrate transformation toughening.

W. Rieger: What is the reason behind making at 1.7 mol% (tetragonal) Y-TZP as the more industrially tested composition is the 3 mol% Y_2O_3 composition. Can you comment on that ?

J. Adair: The 1.7 mole percent was the result of unexpected greater solution binding of the complexing agent, bicine, with the yttrium ion. As a consequence, the targeted concentration of 3.0 mole percent was not reached. However, we believe that the most interesting material to come out of our work is undoped, tetragonal ZrO_2. Preliminary sintering studies have indicated that the tetragonal phase is maintained at least up to 900°C and grain sizes at $\sim$ 50 nm. Certainly, we expect that there will be a critical grain size that displays room temperature transformation toughening. It is our intent to determine the loci of grain size and transformation toughening temperature in the undoped tetragonal, nanoscale zirconia system.

P. Sajgalik: Chemico-mechanical treatment resulted in fine, agglomerated particles. Did you measure the isoelectric point after this treatment? In other words, is isoelectric point size dependent?

J. Adair: The isoelectric point is probably not size dependent at least for the systems we have evaluated, including: $BaTiO_3$ (60 nm); ZrO_2 (8 nm); α-Al_2O_3 (40 nm), and the agglomerated TiO_2 (primary size 40 nm but agglomerated size of $\sim$ 1.5 μm). However, your observation has great merit and we will check the IEP of the well milled titania.
In more several terms, we believe that the IEP is not affected so much as the magnitude of the zeta potential. It is believed by our modeling at the current time that the higher solubility levels of nanoscale particles leads to greater specific site masking both by neutral species and ionic strength effects leading to generally lower zeta potential magnitudes.

S. Barinov: What kind of calcium phosphate compound did you use to prepare envelopes for drug delivery systems?

J. Adair: The hollow envelope can be fabricated by precipitation from a solution containing metasilicate and calcium phosphate. The metasilicate as Na_3SiO_3, and the Ca^{2+} as $CaCl_2$.$2H_2O$ and the PO_4^{3-} as NaH_2PO_4.

L. Hench: Please comment on the effect of nanoscale particles on the structure of water at the particle interface. Will highly structured water form strong polar bridges between nano-particles?

J. Adair: The answer needs to be addressed from two perspectives : external nanoparticle surfaces and the role of water in the internal surface of the nanocomposite particles that were presented in my talk.

External:

Within particle assemblages where surface to surface crowding takes place, the role of water is critical. Some of our analyses are analogous to the water hydration sphere present on ions in aqueous solution, particularly cations such as Al^{3+}, Fe^{3+} and so forth.
The analogue to surface structure and ions present at surfaces is the direct association of water through both hydrolysis reactions, but perhaps more ubiquitously through hydration, hemi – micellular water molecules at cationic surface sites. If this hypothesis that water dictates the metal hydration sphere formation and interacts most strongly with cationic surface sites, then dispersion of nanoscale particles would be most efficient under the acidic conditions that favor the presence of metal ions on metal oxide particle surfaces. This hypothesis is consistent with our experimental finding that chemically aided

milling is most efficient at low pH conditions.
A last point is the possible role of water in surface reactions. We have seen that the formation of oxygen bridges in the alumina system controls the initial stages of agglomerate structures. This finding is analogous to the esterification reactions observed by Hench *et al*, D.R. Uhlmann and others during hydrolysis of metal organic precursors to the sol-gel formation of metal hydroxy oxides. We believe that within a very short time in contact, nanoparticles bond via bridging oxygens that are formed, at least in part, by the presence of water. Our infra-red analyses of commercial powders and MO calculations on the Al-O-H_2O systems are consistent with an adsorption band at 1355 cm^{-1} indicating the presence of the bridging oxygens between alumina clusters.

Internal cavity :

The presence of an external cavity at the nanoscale in nanocomposite particle is possible. The negative curvatures in cavities with diameters around 5 nm lead to a variety of possible effects including: quantum confinement, enhanced adsorption of species, and general breakdown of treating the solution as a continuum. We also believe that during the course of irradiation of the typical fluorescent with conjugated (i.e., multiple double bonds) that activated states such as free radicals, carbonium ions and/or carbanions can lead to chemical bonding between the molecule and the surrounding inorganic matrix leading to more rigid and greater quantum yield in the emission spectra. The quantum confinement effects lead to an enhancement of photonic transitions due to excitonic fluctuations particularly if the shell material is a dielectric. Pinkus at UCSB showed that polymer molecules have enhanced adsorption at surfaces with negative curvature. The presence of fluorescent molecules in the quantum cavity of a nanocomposite particle leads to considerable attenuation of the optical emission spectra. The attenuation of the emission spectra of the quantum confined fluorescent molecule is consistent with the proposed quantum confinement and the enhanced adsorption.
The last aspect of the features of the negative curvature quantum cavities is the role of solvent, especially water. After 30 or so years of controversy, there is no doubt that water can order and associate at surfaces. However, the properties much less a basic understanding of the impact of structural or viscinal water at the solid-solution interface and with respect to interaction energies are not currently understood. However, properties such as the dielectric constant, polar nature of water, etc. should be profoundly affected in the quantum cavity. These are currently topics of much research, continued controversy, and discussion.